Plk1 regulates contraction of postmitotic smooth muscle cells and vascular homeostasis

Guillermo de Cárcer,[1,*] Paulina Wachowicz,[1] Sara Martínez-Martínez,[2,3] Jorge Oller,[2,3] Nerea Méndez-Barbero,[2] Beatriz Escobar,[1] Alejandra González-Loyola,[1] Tohru Takaki,[4] Aicha El Bakkali,[1] Juan A. Cámara,[5] Luis J. Jiménez-Borreguero[3,6], Xosé Bustelo,[8] Marta Cañamero,[9,10] Francisca Mulero,[5] María de los Ángeles Sevilla,[7] María Jose Montero,[7] Juan Miguel Redondo[2,3,*], and Marcos Malumbres[1,*]

[1] *Cell Division and Cancer Group, Spanish National Cancer Research Centre (CNIO), E-28029, Madrid, Spain*

[2] *Gene Regulation in Cardiovascular Remodelling and Inflammation Group, Spanish National Cardiovascular Centre (CNIC), E-28029 Madrid, Spain*

[3] *Centro de Investigaciones Biomédicas en RED (CIBERCV), Spain*

[4] *London Research Institute, London EC1V 4AD, United Kingdom*

[5] *Molecular Imaging Unit, Spanish National Cancer Research Centre (CNIO), E-28029 Madrid, Spain*

[6] *Spanish National Cardiovascular Centre (CNIC), and Hospital de la Princesa, Madrid, Spain*

[7] *Department of Physiology and Pharmacology, University of Salamanca; Biomedical Research Institute of Salamanca (IBSAL), 37007 Salamanca, Spain; and Centro de Investigación Biomédica en Red de Cáncer (CIBERONC), Spain*

[8] *Centro de Investigación del Cáncer de Salamanca, Univ. Salamanca-CSIC, E-27007 Salamanca, and Centro de Investigación Biomédica en Red de Cáncer (CIBERONC), Spain*

[9] *Comparative Pathology Unit, Spanish National Cancer Research Centre (CNIO), E-28029 Madrid, Spain*

[10] Present Address*: Roche Pharma Research and Early Development, Roche Innovation Center Munich, 82377 Penzberg, Germany*

* Correspondence to:

M. Malumbres (malumbres@cnio.es), Centro Nacional de Investigaciones Oncológicas (CNIO); Melchor Fernández Almagro 3, E-28029 Madrid, Spain. Tel. +34 91 732 8000; Fax +34 91 732 8033.

G. de Cárcer (gcarcer@cnio.es), Centro Nacional de Investigaciones Oncológicas (CNIO); Melchor Fernández Almagro 3, E-28029 Madrid, Spain. Tel. +34 91 732 8000; Fax +34 91 732 8033.

J. M. Redondo (jmredondo@cnic.es), Centro Nacional de Investigaciones Cardiovasculares (CNIC); Melchor Fernández Almagro 3, E-28029 Madrid, Spain. Tel. +34 91 453 1200; Fax +34 91 453 1265.

ABSTRACT

Polo-like kinase 1 (Plk1), an essential regulator of cell division, is currently undergoing clinical evaluation as a target for cancer therapy. We report an unexpected function of Plk1 in sustaining cardiovascular homeostasis. *Plk1* haploinsufficiency in mice did not induce obvious cell proliferation defects but resulted in arterial structural alterations, frequently leading to aortic rupture and death. Specific ablation of *Plk1* in (VSMC) led to reduced arterial elasticity, hypotension, and an impaired arterial response to angiotensin II *in vivo*. Mechanistically, we found that Plk1 regulates angiotensin II-dependent activation of RhoA and actomyosin dynamics in VSMCs in a mitosis-independent manner. This regulation depends on Plk1 kinase activity, and administration of small molecule Plk1 inhibitors to angiotensin II-treated mice led to reduced arterial fitness and an elevated risk of aneurysms and aortic rupture. Thus, a partial reduction of Plk1 activity that does not block cell division can nevertheless impair aortic homeostasis, a finding with potentially important implications for current approaches aimed at Plk1 inhibition for cancer therapy.

Current therapeutic efforts to treat tumors include strategies aimed at inhibiting the activity of cell cycle enzymes such as mitotic kinases. Polo-like kinase 1 (Plk1) is an essential protein kinase, originally discovered in *Drosophila*[1,2], that plays multiple roles in centrosome maturation and separation, DNA replication, chromosome segregation, and cytokinesis[3-5]. Chemical inhibition or RNA interference targeting Plk1 results in prometaphase arrest due to monopolar spindles or misaligned chromosomes, as well as specific defects during cytokinesis[4,6,7]. However, the functional roles of this kinase have been mostly characterized in cellular systems and its physiological relevance in mammals is largely unknown.

Plk1 is overexpressed in human tumors and its expression level has prognostic value, leading to the development of a number of small-molecule inhibitors that are currently in clinical trials for cancer therapy[4,8,9]. One of these inhibitors, volasertib (BI6727), recently received a Breakthrough Therapy designation by the FDA due to its significant therapeutic effect in acute myeloid leukemia (AML) patients[10,11].

We show here that both *Plk1* mutant mice and mice treated with Plk1 inhibitors display an unexpected defect in arterial structure, leading to aortic rupture and lethality. We demonstrate that Plk1 is specifically required in postmitotic vascular smooth muscle cells (VSMCs) for RhoA activation and vasoconstriction. The requirement of Plk1 for normal arterial structure has implications for the clinical use of Plk1 inhibitors.

RESULTS

Cardiovascular defects in *Plk1*(+/–) mice

Plk1 is an essential gene in the mouse and homozygous genetic ablation of *Plk1* in the germline [*Plk1*(–/–)] results in early embryonic lethality[12,13]. We recently generated a

conditional knockout allele [*Plk1*(lox)] in which exon 2 of the *Plk1* gene is flanked by loxP sites[13,14]. To study the physiological consequences of *Plk1* inactivation in adult mice, we intercrossed *Plk1*(lox/lox) conditional knockout mice with knockin mice expressing a ubiquitously-expressed, tamoxifen-inducible Cre recombinase (a Cre-estrogen receptor (ERT) fusion protein[15]). We injected young (3-month old) *Plk1*(lox/lox);Cre-ERT and control mice with tamoxifen intraperitoneally (i.p.) to activate Cre, leading to excision of *Plk1* exons and thereby generating the *Plk1*(Δ) allele. All treated *Plk1*(Δ/Δ) mice died within 10 days, whereas control mice were alive for the duration of the experiment (Fig. 1a). Plk1-deficient mice rapidly lost weight (Fig. 1b) and had an altered architecture of the intestinal mucosa (Fig. 1c), suggesting that defective nutrient absorption was the primary cause of death in these mice. The intestinal mucosa showed a high number of cells with aberrant mitosis, as detected by phospho(S10)-histone H3 staining (Fig. 1c,d). Lack of Plk1 also resulted in dramatic loss of cellularity in the bone marrow and a significant alteration in blood cell populations (Supplementary Fig. 1a,b), consistent with an essential role of Plk1 in rapidly proliferating cells.

Due to the rapid lethality after complete *Plk1* ablation, we next focused our attention on *Plk1*(+/–) heterozygous mice. Although these mice were viable and fertile with no obvious defects in proliferative tissues (Supplementary Fig. 1c-e), the viability of these mice was significantly compromised, as ~50% of *Plk1*(+/–) mice died by 1.5-years of age (Fig. 1e). Unexpectedly, in about half of these cases, *Plk1*(+/–) mice died as a consequence of massive hemorrhaging in the thoracic or abdominal cavities. Histopathological analysis identified aortic dissection as the main cause of death (Fig. 1f and Supplementary Table 1). Aortic sections from *Plk1*(+/–) mice showed features of media degeneration, including elastic fiber fragmentation and disorganization, as well as

accumulation of mucopolysaccharides (Fig. 1f,g and Supplementary Fig. 2a). Despite no significant differences in blood pressure when compared to wild-type *Plk1*(+/+) littermates (Supplementary Fig. 2b), *Plk1*(+/–) mice showed aortic wall thickening (Supplementary Fig. 2c). Fine-structure analysis by transmission electronic microscopy confirmed an abnormal organization of elastic fibers and vacuolization of smooth muscle cells in the aorta (Supplementary Fig. 2a). Notably both the ascending and descending thoracic and abdominal aortas of *Plk1*(+/–) mice showed a significant dilation of the internal diameter (Fig. 1h and Supplementary Fig. 2d). Finally, total RNA was extracted from the aortas of 3-5-month-old *Plk1*(+/–) and *Plk1*(+/+) mice and we performed microarray analysis to compare gene expression. *Plk1*(+/–) aortas were characterized by a significant downregulation of genes involved in muscle and cardiovascular function, energy production, actin cytoskeleton dynamics, and the Rho-mediated signaling pathway (Supplementary Fig. 2e and Supplementary Tables 2-3).

Plk1 activity is required for vascular contractility

Plk1 is expressed mostly in proliferating tissues[16] (Supplementary Fig. 3a,b), raising questions about the importance of this protein in vascular function in adult mammals. An initial analysis of data available in public databases indicated that *Plk1* is expressed in the aorta, and that *Plk1* mRNA is more abundant in the aorta of hypertensive than normo- or hypotensive mice (Supplementary Fig. 3c). We therefore examined Plk1 expression in adult (3 month old) mice in a model of angiotensin II (AngII)-induced hypertension. We did not detect Plk1 protein in aortas from control, untreated mice by either immunoblotting or immunohistochemistry (Supplementary Fig. 3b,d). However, a significant but transient increase in *Plk1* mRNA and protein levels was observed 3-6 days after treatment with AngII (Supplementary Fig. 3d-f). This treatment did not result

in increased levels of the proliferation marker Ki67 or mitotic phosphorylation of histone H3 (Supplementary Fig. 3g), indicating that transcriptional induction of Plk1 was not a consequence of increased cell cycle entry.

To test the physiological requirement of Plk1 in VSMCs and in arterial function, we specifically ablated *Plk1* in VSMCs by intercrossing *Plk1*(lox/lox) mice with SM22-Cre transgenic mice expressing tamoxifen-inducible Cre recombinase under the control of the mouse *Tagln* (transgelin; smooth muscle protein 22-alpha) promoter[17]. After tamoxifen treatment, these mice (referred to as *Plk1*(Δ/Δ)^{SM} mice) showed efficient excision of *Plk1* in the aorta but not in other tissues such as heart (Fig. 2a), and this gene excision in the aorta correlated with significantly diminished aortic *Plk1* transcript levels (Fig. 2b). After 4 months on a tamoxifen-supplemented diet, 7-8-month-old *Plk1*(Δ/Δ)^{SM} mice had dilated ascending aortas (Fig. 2c) and were hypotensive (Fig. 2d) when compared to *Plk1*(lox/lox) mice fed with tamoxifen in the absence of the SM22-Cre allele (referred to as *Plk1*(lox/lox) mice). *Plk1*(Δ/Δ)^{SM} mice also displayed reduced aortic elasticity, as assessed using isolated aortic rings in a myograph (Fig. 2e). Similarly, the contractile response of aortic rings from *Plk1*(Δ/Δ)^{SM} mice to AngII or phenylephrine was defective (Fig. 2f), and mesenteric arteries from these mice showed a significantly reduced response to phenylephrine, but not to AngII, (Supplementary Figure 4a).

We next tested the impact of VSMC-specific *Plk1* ablation on AngII-induced hypertension. AngII treatment induced *Plk1* mRNA expression in control but not *Plk1*(Δ/Δ)^{SM} mice (Supplementary Fig. 4b), and induced a strong increase in blood pressure in control mice, whereas this effect was much more limited in *Plk1*(Δ/Δ)^{SM} mice (Fig. 2g). AngII-induced cardiac hypertrophy was also less severe in *Plk1*(Δ/Δ)^{SM}

than in control mice (Fig. 2h); this effect correlated with smaller increases in the heart wall thickness (Fig. 2i) and cardiomyocyte cross-sectional area (Fig. 2j). Interestingly, *Plk1*(Δ/Δ)^{SM} mice had a larger internal aortic diameter than control mice with or without AngII treatment (Supplementary Fig. 4c). More importantly, *Plk1* ablation resulted in a significant increase in the number of elastic fiber breaks as compared to control mice (Fig. 2k), as we previously observed in *Plk1*(+/–) mice. Together, these data suggest that Plk1 deficiency in VSMCs results in a cell autonomous defect characterized by structural defects in the tunica media of the aorta, reduced elasticity and a defective response to AngII.

Plk1-deficient VSMCs have an impaired RhoA pathway

To study the mechanistic relevance of Plk1 in vascular cells, we next generated VSMC cultures in which the *Plk1* gene could be conditionally ablated. To avoid the possibility that ablation of *Plk1* would cause mitotic defects, VSMCs isolated from *Plk1*(lox/lox) mice were arrested in G0 by culture in low serum (0.1% FBS) and confluency, and then transduced by adenovirus expressing Cre recombinase, thereby generating a *Plk1* null allele [*Plk1*(Δ)] in quiescent cells (Fig. 3a). Two days later, cells were analyzed either in G0 or in early G1, at time points from 2–10 h after the addition of lysophosphatidic acid (LPA) or Angiotensin II (AngII) to rule out mitotic defects after Plk1 ablation (Supplementary Fig. 5a,b). Six hours after induction with LPA, control cells showed an elongated or polygonal morphology with well-defined actin stress fibers, whereas *Plk1*(Δ/Δ) cells had a more rounded shape with fewer actin fibers (Fig. 3b,c and Supplementary Fig. 5c). Treatment of serum-starved cells in G0 with AngII or LPA induces the formation of stress fibers through activation of RhoA and subsequent phosphorylation of myosin light-chain (MLC)[18]. Lack of Plk1 resulted in impaired

188 phosphorylation of MLC and MYPT1 (Fig. 3d and Supplementary Fig. 5c) and
189 inefficient activation of RhoA (Fig. 3e). We observed similar defects in interphase wild-
190 type VSMCs when Plk1 was chemically inhibited using either of two different small-
191 molecule kinase inhibitors, BI2536 and GW843682X (Fig. 3f,g and Supplementary Fig.
192 5b-d), indicating that these alterations are not an artefactual consequence of genetic
193 modification of the *Plk1* locus, but rather due to deficient Plk1 activity. The Plk1
194 inhibitor BI2536 was also efficient in preventing AngII- or phenylephrine-induced
195 contraction in aortic rings (Figure 3h) and in mesenteric arteries (Supplementary Fig.
196 5e).

197 To determine the relevance of RhoA signaling downstream of Plk1, we repeated
198 these assays using Y27632, a specific inhibitor of RhoA-associated coil kinase (ROCK),
199 or using VSMCs expressing a constitutively-active form of RhoA (the Q63L mutant).
200 ROCK inhibition resulted in effects on stress fiber formation and cell morphology (Fig.
201 3i,j), as well as on MLC phosphorylation (Supplementary Fig. 5b), that were similar to
202 those observed in *Plk1*-null cells. Notably, expression of RhoA Q63L rescued the
203 response of Plk1-deficient cells to LPA (Fig. 3i,j) and to AngII (Supplementary Fig. 5f),
204 suggesting that the morphological and functional alterations induced by Plk1 inhibition
205 are largely due to defective activation of the RhoA GTPase.

206 **Plk1 modulates RhoA activity in an Ect2-dependent manner**

207 We next investigated the molecular mechanism linking Plk1 and RhoA. RhoA is a small
208 GTPase activated by guanine exchange factor (GEF)-mediated GDP/GTP exchange.
209 Several RhoGEFs have been implicated in actin dynamics in VSMCs, including
210 p115GEF (also known as ArhGEF1; ref. [19]), LARG (ArhGEF12; ref. [20]), p63RhoGEF
211 (ref. [21]) and PDZ-RhoGEF (ref. [22]). On the other hand, several RhoGEFs, such as

212 epithelial cell transforming sequence 2 (Ect2) and MyoGEF, have been proposed to
213 regulate RhoA activity during cytokinesis, in which RhoA activation is locally required
214 for the positioning and assembly of the cytokinetic apparatus and acto-myosin
215 contraction at the mitotic furrow (reviewed in ref. [6]).

216 We first tested the expression of each of these GEFs in the context of
217 hypertension. Inspection of data in public repositories showed that, similarly to *Plk1*,
218 *Arhgef1* (encoding p115GEF) and *Ect2* transcripts were more abundant in aortas from
219 hypertensive mice as compared to normo- or hypotensive mice; however, there was no
220 significant increase in the transcripts encoding MyoGEF, LARG, PDZ-RhoGEF or p63-
221 RhoGEF (Supplementary Fig. 6). We verified these data using RNA from aortas of
222 AngII-treated mice. AngII treatment led to an increase in *Ect2, Plekhg6* (encoding
223 MyoGEF) and *Arhgef1* mRNA levels, as assessed 6 days after treatment (Fig. 4a),
224 whereas *Arhgef12* (encoding LARG) mRNA levels were not affected, in agreement with
225 published data suggesting that LARG activity is responsive mainly to salt-induced
226 hypertension[20]. To test the involvement of these GEFs in the regulation of VSMC
227 cytoskeletal dynamics, we tested the effect of RNA interference-mediated GEF
228 depletion on the cell roundness factor. When either Ect2 or p115GEF were depleted,
229 VSMCs did not polarize properly in the presence of LPA (Fig. 4b, c), whereas LARG or
230 MyoGEF depletion had no effects. Similar studies using AngII showed that Ect2 is a
231 critical factor for both AngII-induced morphological changes (Fig. 4d) and MLC
232 phosphorylation (Fig. 4e). Thus, activation of RhoA by AngII may be mediated not only
233 by p115GEF but also by Ect2, indicating that Ect2 may have cell-cycle-independent
234 functions in controlling RhoA activity.

235 The recruitment of Ect2 to the cleavage furrow during cytokinesis depends on
236 Plk1-mediated phosphorylation of the Rho GTPase activating protein (GAP) RacGAP1

(also known as MgcRacGAP or HsCyk4); RacGAP1 therefore counterintuitively functions as a RhoA activator via Ect2 recruitment[23-27]. *Racgap1* mRNA expression was significantly induced in aortas from AngII-treated mice (Fig. 4a), and RacGAP1 depletion in VSMCs led to similar defects in cell roundness (Fig. 4b,d) and phosphorylation of MLC (Fig. 4e) to those observed after Plk1 inactivation.

During cytokinesis, Plk1 is known to phosphorylate several sites in the N-terminal domain of RacGAP1, thereby generating a docking site for the tandem BRCT repeats of Ect2 (refs. [25,26]). We found that one of these N-terminal domain residues of RacGAP1, Ser170, was phosphorylated 10-30 min after treatment of quiescent VSMCs cells with LPA or AngII (Fig. 4f,g), concomitantly with phosphorylation of MLC (used as a read-out of RhoA pathway activation). Notably, phosphorylation of both RacGAP1 and MLC were impaired by Plk1 inhibition with BI2536. Moreover, inhibition of Plk1 with BI2536 prevented the binding of Ect2 to RhoA in quiescent VSMCs 20 min after stimulation with LPA (Fig. 4h). Plk1 activity was also required for the binding of wild-type RacGAP1 to RhoA, whereas a RacGAP1 mutant with four phospho-mimetic (Ser-to-Asp) mutations at positions Ser149, Ser159, Ser164 and Ser170 (4D mutant; ref. [26]) bound to RhoA independently of Plk1 activity (Fig. 4h).

Activation of RhoA by Ect2 depends on both Plk1 and atypical PKC

In interphase cells, Plk1 is localized to both the cytoplasm and nucleus, without any obvious concentration in cellular membranes[6]. RacGAP1 and Ect2 are mostly nuclear, although RacGAP1 can also localize to microtubule-dense regions in the cytoplasm[28], as well as to cell-cell contact regions in the plasma membrane[29]. We therefore tested whether these proteins are re-distributed upon stimulation of the RhoA pathway in VSMCs. Upon treatment with AngII, endogenous Plk1 was clearly enriched in cell

protrusions that were also enriched for phosphorylated MLC (Fig. 5a). A similar re-distribution of Plk1 was observed in LPA-stimulated VSMCs expressing a GFP-Plk1 fusion protein (Supplementary Figure 7a). We could not study effects on the localization of endogenous Ect2 protein, because available antibodies are of insufficient quality. However, in VSMCs expressing a GFP-Ect2 fusion protein, a pool of GFP-Ect2, which was mostly nuclear-localized prior to stimulation, shuttled to the cytoplasm at ~10 min after LPA treatment (Fig. 5b and Supplementary Fig. 7a). This cytoplasmic pool of Ect2 localized preferentially to cell protrusions and remained in these protrusions for at least the following 2 h. We did not observe any substantial changes in the subcellular localization of a GFP-RacGAP1 fusion protein in response to LPA (data not shown). These results suggest that both Plk1 and Ect2 are dynamically redistributed in the cell upon stimulation of the RhoA pathway.

Since Plk1 has been proposed to phosphorylate Ect2 during cytokinesis[30], we analyzed effects of LPA on the phosphorylation of specific Ect2 residues by mass spectrometry. In HEK293 cells, we identified two Ect2 residues (Thr327 and Ser335) specifically phosphorylated after treatment with LPA. It is worth mentioning that we did not find phosphorylation at either of the sites reported to be phosphorylated by Cdk1 (Thr341 and Thr412), which are required for Ect2 function during cytokinesis[31]. Notably, Thr327, but not Ser335, is a putative PDB-binding site, as it is adjacent to a proline residue (Supplementary Fig. 7b,c), and previous reports have demonstrated that the atypical protein kinase C (aPKC) PKCι can phosphorylate Ect2 at this threonine residue in cancer cells and thereby regulate its nuclear export[32]. We therefore hypothesized that binding of Ect2 to Plk1 and RhoA could be modulated by aPKC–dependent phosphorylation. Indeed, we found that Ect2 efficiently bound to Plk1 20 minutes after LPA induction, and that this binding was substantially impaired by

286 treatment with the PKC inhibitor Go6983 (Fig. 5c). This inhibitor also prevented
287 elongation of VSMCs, an effect similar to that of the ROCK inhibitor Y27632 or *Plk1*
288 ablation (Fig. 5d); however, Go6983 had no significant effect in Plk1-deficient cells
289 (Supplementary Fig. 7d), suggesting a critical role of aPKC in the binding of Ect2 to
290 RhoA and subsequent changes in cell morphology. We tested the requirement for Plk1,
291 ROCK and aPKC activity in arterial contraction in an independent manner using
292 specific Plk1, ROCK or aPKC inhibitors (BI2536, Y27632 and GO6983, respectively)
293 in aortic rings isolated from wild-type mice. Phenylephrine-induced contraction of these
294 rings was significantly reduced by each of these inhibitors, with the ROCK inhibitor
295 showing the strongest effect (Supplementary Fig. 7e).

296 We next tested the importance of Ect2 Thr327 phosphorylation by generating a
297 phosphorylation-resistant mutant, in which Thr327 was mutated to Ala. RhoA-17A-
298 coated-beads efficiently pulled down wild type GFP-Ect2 but not mutant Ect2 T327A,
299 from lysates of LPA-treated HEK293 cells (Fig. 5e). Similarly, the Ect2-T327A mutant
300 displayed lower affinity for the Plk1 Polo-box domain (Plk1-PBD) compared to wild
301 type Ect2 (Fig. 5f), suggesting that Plk1 can recognize and bind Ect2 when it is
302 phospho-primed at the Thr327 residue. Moreover, whereas wild-type Ect2 but not the
303 Ect2-T327A mutant could efficiently rescue the defect in cell elongation caused by Ect2
304 deficiency (Fig. 5g). However, Ect2-T327A was able to rescue cell division defects
305 caused by Ect2 deficiency (Supplementary Fig. 7f), suggesting that phosphorylation of
306 Ect2 at T327 is dispensable during mitosis or cytokinesis but participates in cytoskeletal
307 re-arrangements during interphase.

308 We also analyzed whether Plk1-mediated phosphorylation of Ect2 could
309 contribute to the activation of RhoA. We generated an Ect2 mutant, designated the 14A
310 mutant, containing alanine substitutions at all 14 D/E/N-X-S/T-φ sites (putative sites of

Plk1-mediated phosphorylation, where X represents any amino acid residue and φ denotes a hydrophobic residue) of Ect2. This mutant protein was phosphorylated by recombinant Plk1 *in vitro* to a much lower extent than was wild-type Ect2 (Supplementary Fig. 7g,h). However, unlike the T327A mutant, the 14A mutant displayed normal binding to RhoA (Fig. 5e). In addition, we did not detect phosphorylation of any of these 14 sites after stimulation of HEK293 expressing GFP-Ect2 with LPA (data not shown). Thus, although we cannot rule out the possibility that Ect2 is phosphorylated by Plk1, we did not find evidence for Ect2 regulation by direct phosphorylation by Plk1. Taken together, these data suggest that Ect2 phosphorylation at Thr327 by aPKC mediates the interaction of Plk1 and Ect2, thereby promoting RhoA activity and actin cytoskeleton dynamics in interphase VSMCs.

Plk1 inhibitors induce aortic dilation and defective vascular function

In view of the effects Plk1 inhibition on VSMC function in vitro, we next tested whether Plk1 inhibition would affect vascular homeostasis in adult mice *in vivo.* We treated wild-type mice with 15 mg/kg volasertib, the Plk1 inhibitor that has advanced furthest in the clinic, for 1 month, and then with AngII plus volasertib for an additional 4 weeks (Fig. 6a). At this low dose, volasertib treatment did not induce weight loss or reduce peripheral blood cell counts, suggesting that it did not cause major defects in cell proliferation (Supplementary 8a,b). However, consistent with the phenotype of Plk1-deficient aortas, aortic rings isolated from mice treated with volasertib for eight weeks treatment had defective elasticity (Fig. 6b). Although volasertib treatment induced an initial and transient small increase in blood pressure (Supplementary Fig. 8c), the hypertension that is typically induced by AngII treatment was significantly impaired by

335 Plk1 inhibition (Fig. 6c), consistent with the effect of VSMC-specific Plk1 deficiency in
336 *Plk1*(Δ/Δ)^{SM} mice. Treatment with volasertib (Fig. 6d) or GW843682X (Supplementary
337 Fig. 8d-f) reduced AngII-induced cardiac hypertrophy, as was also observed in the
338 genetic model.

339 Ultrasound analysis of wild-type mice treated with volasertib for 1 month
340 showed significant dilation of the abdominal aorta in the suprarenal region
341 (Supplementary Fig. 8g). This effect was more pronounced after volasertib treatment for
342 2 months, especially in the ascending aorta and descending aorta close to the diaphragm
343 (Fig. 6e). Moreover, treatment with either volasertib or AngII significantly increased
344 elastic fiber fragmentation when compared to untreated mice, and combined treatment
345 with volasertib and AngII had greater effects than treatment with either alone (Fig. 6f).
346 Strikingly, combined treatment with AngII and volasertib induced aneurysms (4/8 mice)
347 and aortic dissections (3/8 mice; Fig. 6g), whereas these were never observed after
348 treatment with either of these agents alone (0/6 AngII- and 0/5 volasertib-treated mice).
349 Together, these results suggest that Plk1 participates in VSMC function *in vivo* in a
350 manner dependent on its kinase activity, and that sustained treatment with Plk1
351 inhibitors may result in altered AngII responses and pronounced vascular defects.
352

353 **DISCUSSION**

354 Plk1 is essential for mitosis in all eukaryotes where its function has been tested[5-7].
355 Whereas whole-body ablation of Plk1 is highly toxic in adult mice, *Plk1*(+/–) mice
356 develop normally and cells derived from these heterozygous mutants do not display
357 obvious defects in cell proliferation[13]. However, we found that *Plk1* haploinsufficiency
358 results in a syndrome of cardiovascular defects and premature lethality, due primarily to

aortic rupture. The structure of the aorta is disrupted in *Plk1*(+/–) mice, and transcriptional profiling suggests that these defects may arise, at least in part, from abnormalities in the RhoA pathway and in the actomyosin cytoskeleton. Although Plk1 is known to be highly expressed in proliferative tissues[16], we found that Plk1 is also expressed at low levels in the aorta and that AngII treatment of mice led to transcriptional induction of Plk1 and other members of the RhoA pathway. Specific ablation of *Plk1* in VSMCs resulted in stiffening of the aorta and a defective response to AngII *in vivo*, as well as defective RhoA-dependent actomyosin cytoskeleton dynamics in VSMCs *in vitro***.** Expression of constitutively activated RhoA rescued the defective actomyosin dynamics, suggesting that RhoA is a major target of Plk1 in these cells.

The control of myosin contractility by Polo-like kinases is conserved through evolution[6,33-35]. During cytokinesis, Plk1 is required to generate an area in which RhoA is active and where ingression of the cleavage furrow originates. Plk1 modulates RhoA function during cytokinesis through direct phosphorylation of the RhoA exchange factor Ect2, although the precise residues that are phosphorylated remain elusive[26,30]. Recent data have established a mechanism in which Plk1 phosphorylates the GTPase-activating protein RacGAP1, which subsequently recruits Ect2 to the area of the cleavage furrow, thereby promoting RhoA activation in the middle of the cell[23-26].

Despite this previously established cell-cycle-dependent connection between Plk1 and RhoA, our finding that Plk1 is haploinsufficient for vascular homeostasis was unexpected. Different GEFs have been suggested to play a role in the activation of RhoA in smooth muscle cells, including LARG [20], p115RhoGEF [19], p190RhoGEF and GEF-H1 [36]. In particular, in mice deficient for p115GEF, RhoA is not activated upon AngII treatment[19], whereas in mice deficient for LARG, RhoA is not activated in a model of salt-induced hypertension[20]. Although the role of the GEF Ect2 in RhoA

activation in these settings has not been established, *Ect2* expression is upregulated in mice with AngII-induced hypertension[37]. We observed that the mRNA levels of *Plk1* and *Racgap1*, in addition to those of *Ect2*, are elevated in mice with AngII-induced hypertension. Despite the fact that Ect2 is mostly localized to the nucleus, Ect2 has been implicated in cell polarity[38], is able to activate Rho signaling at the zonula adherens in epithelial cells[29], and can shuttle from the nucleus to the cytoplasm after phosphorylation by either atypical-PKC (aPKC)[39] or Cdk1[40,41]. Moreover, PKC enzymes have been proposed to mediate RhoA-dependent alteration of vascular physiology, although the underlying mechanisms are not fully understood[42,43]. Our data suggest that aPKC may contribute to the regulation of actomyosin dynamics in VSMCs through the phosphorylation and nuclear export of Ect2. The residue of Ect2 phosphorylated by aPKC, Thr327, is located in the so-called "hinge" domain of Ect2, very close to the two central NLS sequences and to sites phosphorylated by Cdk1. During mitosis, phosphorylation of Ect2 by Cdk1 at T412 regulates the binding of Ect2 to Plk1, such that the Ect2 T412A mutant does not exhibit a strong association with Plk1[30]. The observation that the Ect2 T327A mutant cannot be exported from the nucleus[32] suggests that aPKC-dependent phosphorylation at Thr327 determines its nuclear export[32] and binding to Plk1. Thus, both Cdks and aPKC may function to prime Ect2 for Plk1 binding, during mitosis and during interphase, respectively.

The presence of elastic fiber breaks, aneurysms, and aortic dissections in *Plk1*(+/–) and *Plk1*$(\Delta/\Delta)^{SM}$ mice, as well as in wild-type mice treated with volasertib, indicate further functions of Plk1 in the maintenance of aortic structure. AngII treatment exacerbated the induction of elastic fiber breaks and aneurysms by Plk1 inhibition using volasertib. As we did not observe these phenotypes after specific ablation of Plk1 in VSMCs, we speculate that either Plk1 depletion in the *Plk1*$(\Delta/\Delta)^{SM}$ model is incomplete

409 or that volasertib has additional effects in other vascular cell types. The role of the
410 Plk1/RhoA axis in the regulation of vascular contractility and homeostasis is consistent
411 with findings that familial forms of thoracic aortic aneurysms and dissections (TAAD)
412 are frequently caused by mutations that affect the structure and function of the
413 contractile unit of medial smooth muscle cells[44,45]. These familial forms of TAAD are
414 typically inherited in an autosomal dominant pattern with variable disease expression[45].
415 Similarly to Plk1 deficiency, loss-of-function mutations in the genes encoding smooth
416 muscle myosin heavy chain (MYH11)[46] or myosin light chain kinase (MLCK)[47] result
417 in impaired myosin contractility and aortic aneurysms and dissections, preferentially
418 affecting the ascending aorta. *Myh11* mutant mice have normal systemic blood pressure;
419 however, VSMCs from these mice have impaired contractility[48] and these mice have an
420 above-normal incidence of aortic aneurysm and dissection in the presence of
421 hypertension[49]. Elevated blood pressure and defective myosin contractility thus
422 cooperate to generate these vascular defects. Targeted deletion of the mouse MLCK-
423 encoding gene, *Mylk*, in VSMCs results in hypotension accompanied by features of
424 medial degeneration of the aorta[47,50]. Moreover, deletion of the counteracting
425 phosphatase (myosin phosphatase target subunit 1) gene, *Mypt1*, results in increased
426 intestinal smooth muscle contractility in response to specific stimuli[51]. Notably, Plk1
427 forms a complex with MYPT1[52], suggesting that Plk1 may have RhoA-independent
428 roles in myosin function. Plk1 can also regulate other cytoskeletal proteins related to
429 cellular contraction, such as vimentin, and may thus have additional roles in cellular
430 contraction, as shown in the airway smooth muscle[53]. Finally, whether Plk1 affects the
431 structure or function of extracellular elastin fibers is an interesting possibility that
432 deserves further investigation.

Plk1 inhibitors are currently in advanced clinical trials for cancer treatment[9,54]. The main adverse effects of these inhibitors that have been reported are hematological alterations such as anemia, neutropenia and thrombocytopenia, as well as gastrointestinal events, which are likely a consequence of the essential role of Plk1 in the cell cycle. A few treated individuals have been reported to experience thromboembolism or phlebitis[55], hemorrhages[56,57] and changes in blood pressure (Clinical trial NCT01121406 and Ref. [58]), although to what extent these adverse events can be ameliorated by changes in dosing or treatment length is unclear at present. Nonetheless, our data suggest a note of caution in the use of Plk1 inhibitors, as they may have cardiovascular side effects, such as hypotension, hemorrhage and aneurysm, especially with extended treatment or with treatment of hypertensive patients.

The observation that *Plk1* haploinsufficiency results in deficient RhoA activation without obvious defects in the cell cycle suggests a stronger requirement for Plk1 activity in the RhoA pathway than in sustaining cell proliferation. As RhoA is a critical mediator of major oncogenic or metastatic pathways[59,60], the use of low doses of Plk1 inhibitors could be considered as an attractive therapeutic strategy to limit the activation of these pathways in cancer cells. A better understanding of the physiological requirements for Plk1 in different tissues, either as an essential cell cycle kinase or as a RhoA regulator, will undoubtedly improve future therapeutic strategies aimed at inhibiting this kinase in human disease.

ACKNOWLEDGEMENTS

We are fully indebted to Keith Burridge (The University of North Carolina at Chapel Hill, NC), Channing J. Der (The University of North Carolina at Chapel Hill, NC), Alan

P. Fields (Mayo Clinic, Jacksonville), Michael Glotzer (University of Chicago, Chicago, IN), Miguel Angel del Pozo (CNIC, Madrid) and Michael Yaffe (The Koch Institute, MIT, Cambridge, MA) for reagents. We thank Alessia Borgia for help with biochemical studies, the ultrasonographers Ana Vanesa Alonso and Lorena Flores, Alicia Peral and Rut Alberca for technical assistance, and Javier Regadera for their advice in mouse echocardiography and pathological samples, and members of the Histopathology and Transgenic Units of the CNIO for excellent technical support. We also thank David Olmos for discussion on the effect of Plk1 inhibitors in the clinic. P.W. and A.G.-L. received fellowships from the Marie Curie activities of the European Commission (Oncotrain programme), and the Spanish Ministry of Economy and Competitiveness (MINECO), respectively. The Molecular Imaging Unit of the CNIO is granted by CENIT (Spanish Centre of studies in technological and industrial transfer) AMIT Project "Advanced Molecular Imaging tehnologies" (TEC2008-06715-C02-1, RD07/0014/2009 to F.M.). Work in J.M.R. lab. was funded by MINECO SAF2015-636333R, and CIBERCV. The Red de Investigación Cardiovascular (RIC) cofunded by FEDER supports the research of J.M.R. and L.J.J.-B. with grants RD12/0042/0022 and RD12/0042/0056, respectively. J.M.R. is also funded by Fundació La Marató TV3 (Grant 20151331). CNIC is supported by MINECO and Pro-CNIC Foundation. M.M. lab was funded by the MINECO (SAF2015-69920-R), Consolider-Ingenio 2010 Programme (SAF2014-57791-REDC), Red Temática CellSYS (BFU2014-52125-REDT), Comunidad de Madrid (OncoCycle Programme; S2010/BMD-2470), Worldwide Cancer Research (WCR #15-0278) and the MitoSys project (HEALTH-F5-2010-241548; European Union Seventh Framework Programme). CNIO and CNIC are Severo Ochoa Centers of Excellence (MINECO awards SEV-2015-0510 and SEV-2015-0505, respectively). The authors have no conflict of interest to declare.

AUTHOR CONTRIBUTIONS

G.d.C. performed most of the cellular and mouse experiments with technical support from B.E. and A.E.B. P.W. generated the Plk1 alleles and performed initial experiments in Plk1 heterozygous mice and VSMCs. S.M.-M., J.O., N.M.-B., L.J.J.-B. and J.M.R. provided intellectual input on the cardiovascular studies and contributed to the phenotypic analysis of the vascular phenotype in mice. A.G.-L. helped with cellular and biochemical assays. J.A.C. and F.M. helped with echocardiography measurements. M.J.M and M.d.l.A.S performed the contractility and elasticity assays in the rings from aortas or the mesenteric arteries. X.B. provided intellectual input for the initial project design and further troubleshooting. T.T. studied the phosphorylation of Ect2 by Plk1. M.C. performed the histopathological analysis. G.d.C and M.M. supervised the project and wrote the manuscript with the help of all the authors.

COMPETING FINANCIAL INTERESTS

The authors declare no competing financial interests.

REFERENCES

1. Llamazares, S., *et al.* polo encodes a protein kinase homolog required for mitosis in Drosophila. *Genes Dev* **5**, 2153-2165 (1991).
2. Sunkel, C.E. & Glover, D.M. polo, a mitotic mutant of Drosophila displaying abnormal spindle poles. *J Cell Sci* **89 (Pt 1)**, 25-38 (1988).
3. Barr, F.A., Sillje, H.H. & Nigg, E.A. Polo-like kinases and the orchestration of cell division. *Nat Rev Mol Cell Biol* **5**, 429-440 (2004).
4. Lens, S.M., Voest, E.E. & Medema, R.H. Shared and separate functions of polo-like kinases and aurora kinases in cancer. *Nat Rev Cancer* **10**, 825-841 (2010).
5. Archambault, V. & Glover, D.M. Polo-like kinases: conservation and divergence in their functions and regulation. *Nat Rev Mol Cell Biol* **10**, 265-275 (2009).
6. Petronczki, M., Lenart, P. & Peters, J.M. Polo on the Rise-from Mitotic Entry to Cytokinesis with Plk1. *Dev Cell* **14**, 646-659 (2008).
7. Taylor, S. & Peters, J.M. Polo and Aurora kinases: lessons derived from chemical biology. *Curr Opin Cell Biol* **20**, 77-84 (2008).
8. Strebhardt, K. & Ullrich, A. Targeting polo-like kinase 1 for cancer therapy. *Nat Rev Cancer* **6**, 321-330 (2006).
9. McInnes, C. & Wyatt, M.D. PLK1 as an oncology target: current status and future potential. *Drug Discov Today* **16**, 619-625 (2011).
10. Dohner, H., *et al.* Randomized, phase 2 trial of low-dose cytarabine with or without volasertib in AML patients not suitable for induction therapy. *Blood* **124**, 1426-1433 (2014).
11. Gjertsen, B.T. & Schoffski, P. Discovery and development of the Polo-like kinase inhibitor volasertib in cancer therapy. *Leukemia* **29**, 11-19 (2015).
12. Lu, L.Y., *et al.* Polo-like kinase 1 is essential for early embryonic development and tumor suppression. *Mol Cell Biol* **28**, 6870-6876 (2008).
13. Wachowicz, P., Fernández-Miranda, G., Marugán, C., Escobar, B. & de Cárcer, G. Genetic depletion of Polo-like kinase 1 leads to embryonic lethality due to mitotic aberrancies. *BioEssays* **38**, S96-S106 (2016).
14. Trakala, M., *et al.* Activation of the endomitotic spindle assembly checkpoint and thrombocytopenia in Plk1-deficient mice. *Blood* **126**, 1707-1714 (2015).
15. Guerra, C., *et al.* Tumor induction by an endogenous K-ras oncogene is highly dependent on cellular context. *Cancer Cell* **4**, 111-120 (2003).
16. Winkles, J.A. & Alberts, G.F. Differential regulation of polo-like kinase 1, 2, 3, and 4 gene expression in mammalian cells and tissues. *Oncogene* **24**, 260-266 (2005).
17. Kuhbandner, S., *et al.* Temporally controlled somatic mutagenesis in smooth muscle. *Genesis* **28**, 15-22 (2000).
18. Loirand, G. & Pacaud, P. Involvement of Rho GTPases and their regulators in the pathogenesis of hypertension. *Small GTPases* **5**, 1-10 (2014).
19. Guilluy, C., *et al.* The Rho exchange factor Arhgef1 mediates the effects of angiotensin II on vascular tone and blood pressure. *Nat Med* **16**, 183-190 (2010).
20. Wirth, A., *et al.* G12-G13-LARG-mediated signaling in vascular smooth muscle is required for salt-induced hypertension. *Nat Med* **14**, 64-68 (2008).
21. Wuertz, C.M., *et al.* p63RhoGEF--a key mediator of angiotensin II-dependent signaling and processes in vascular smooth muscle cells. *FASEB J* **24**, 4865-4876 (2010).
22. Ying, Z., Giachini, F.R., Tostes, R.C. & Webb, R.C. PYK2/PDZ-RhoGEF links Ca2+ signaling to RhoA. *Arterioscler Thromb Vasc Biol* **29**, 1657-1663 (2009).
23. Zhao, W.M. & Fang, G. MgcRacGAP controls the assembly of the contractile ring and the initiation of cytokinesis. *Proc Natl Acad Sci U S A* **102**, 13158-13163 (2005).

24. Petronczki, M., Glotzer, M., Kraut, N. & Peters, J.M. Polo-like kinase 1 triggers the initiation of cytokinesis in human cells by promoting recruitment of the RhoGEF Ect2 to the central spindle. *Dev Cell* **12**, 713-725 (2007).
25. Burkard, M.E.*, et al.* Plk1 self-organization and priming phosphorylation of HsCYK-4 at the spindle midzone regulate the onset of division in human cells. *PLoS Biol* **7**, e1000111 (2009).
26. Wolfe, B.A., Takaki, T., Petronczki, M. & Glotzer, M. Polo-like kinase 1 directs assembly of the HsCyk-4 RhoGAP/Ect2 RhoGEF complex to initiate cleavage furrow formation. *PLoS Biol* **7**, e1000110 (2009).
27. Zhang, D. & Glotzer, M. The RhoGAP activity of CYK-4/MgcRacGAP functions non-canonically by promoting RhoA activation during cytokinesis. *eLife* **4**(2015).
28. Hirose, K., Kawashima, T., Iwamoto, I., Nosaka, T. & Kitamura, T. MgcRacGAP is involved in cytokinesis through associating with mitotic spindle and midbody. *J Biol Chem* **276**, 5821-5828 (2001).
29. Ratheesh, A.*, et al.* Centralspindlin and alpha-catenin regulate Rho signalling at the epithelial zonula adherens. *Nat Cell Biol* **14**, 818-828 (2012).
30. Niiya, F., Tatsumoto, T., Lee, K.S. & Miki, T. Phosphorylation of the cytokinesis regulator ECT2 at G2/M phase stimulates association of the mitotic kinase Plk1 and accumulation of GTP-bound RhoA. *Oncogene* **25**, 827-837 (2006).
31. Hara, T.*, et al.* Cytokinesis regulator ECT2 changes its conformation through phosphorylation at Thr-341 in G2/M phase. *Oncogene* **25**, 566-578 (2006).
32. Justilien, V., Jameison, L., Der, C.J., Rossman, K.L. & Fields, A.P. Oncogenic activity of Ect2 is regulated through protein kinase C iota-mediated phosphorylation. *J Biol Chem* **286**, 8149-8157 (2011).
33. Yoshida, S.*, et al.* Polo-like kinase Cdc5 controls the local activation of Rho1 to promote cytokinesis. *Science* **313**, 108-111 (2006).
34. Ohkura, H., Hagan, I.M. & Glover, D.M. The conserved Schizosaccharomyces pombe kinase plo1, required to form a bipolar spindle, the actin ring, and septum, can drive septum formation in G1 and G2 cells. *Genes Dev* **9**, 1059-1073 (1995).
35. Petersen, J. & Hagan, I.M. Polo kinase links the stress pathway to cell cycle control and tip growth in fission yeast. *Nature* **435**, 507-512 (2005).
36. Guilluy, C., Garcia-Mata, R. & Burridge, K. Rho protein crosstalk: another social network? *Trends Cell Biol* **21**, 718-726 (2011).
37. Cario-Toumaniantz, C.*, et al.* RhoA guanine exchange factor expression profile in arteries: evidence for a Rho kinase-dependent negative feedback in angiotensin II-dependent hypertension. *American journal of physiology. Cell physiology* **302**, C1394-1404 (2012).
38. Liu, X.F., Ishida, H., Raziuddin, R. & Miki, T. Nucleotide exchange factor ECT2 interacts with the polarity protein complex Par6/Par3/protein kinase Czeta (PKCzeta) and regulates PKCzeta activity. *Mol Cell Biol* **24**, 6665-6675 (2004).
39. Justilien, V. & Fields, A.P. Ect2 links the PKCiota-Par6alpha complex to Rac1 activation and cellular transformation. *Oncogene* **28**, 3597-3607 (2009).
40. Matthews, H.K.*, et al.* Changes in Ect2 localization couple actomyosin-dependent cell shape changes to mitotic progression. *Dev Cell* **23**, 371-383 (2012).
41. Suzuki, K.*, et al.* Identification of non-Ser/Thr-Pro consensus motifs for Cdk1 and their roles in mitotic regulation of C2H2 zinc finger proteins and Ect2. *Scientific reports* **5**, 7929 (2015).
42. Liao, D.F., Monia, B., Dean, N. & Berk, B.C. Protein kinase C-zeta mediates angiotensin II activation of ERK1/2 in vascular smooth muscle cells. *J Biol Chem* **272**, 6146-6150 (1997).
43. Pan, J.*, et al.* PKC mediates cyclic stretch-induced cardiac hypertrophy through Rho family GTPases and mitogen-activated protein kinases in cardiomyocytes. *J Cell Physiol* **202**, 536-553 (2005).

44. Lindsay, M.E. & Dietz, H.C. The genetic basis of aortic aneurysm. *Cold Spring Harbor perspectives in medicine* **4**, a015909 (2014).
45. Milewicz, D.M., Regalado, E.S., Shendure, J., Nickerson, D.A. & Guo, D.C. Successes and challenges of using whole exome sequencing to identify novel genes underlying an inherited predisposition for thoracic aortic aneurysms and acute aortic dissections. *Trends in cardiovascular medicine* **24**, 53-60 (2014).
46. Zhu, L., *et al.* Mutations in myosin heavy chain 11 cause a syndrome associating thoracic aortic aneurysm/aortic dissection and patent ductus arteriosus. *Nat Genet* **38**, 343-349 (2006).
47. Wang, L., *et al.* Mutations in myosin light chain kinase cause familial aortic dissections. *American journal of human genetics* **87**, 701-707 (2010).
48. Kuang, S.Q., *et al.* Rare, nonsynonymous variant in the smooth muscle-specific isoform of myosin heavy chain, MYH11, R247C, alters force generation in the aorta and phenotype of smooth muscle cells. *Circ Res* **110**, 1411-1422 (2012).
49. Bellini, C., Wang, S., Milewicz, D.M. & Humphrey, J.D. Myh11(R247C/R247C) mutations increase thoracic aorta vulnerability to intramural damage despite a general biomechanical adaptivity. *Journal of biomechanics* **48**, 113-121 (2015).
50. He, W.Q., *et al.* Myosin light chain kinase is central to smooth muscle contraction and required for gastrointestinal motility in mice. *Gastroenterology* **135**, 610-620 (2008).
51. He, W.Q., *et al.* Altered contractile phenotypes of intestinal smooth muscle in mice deficient in myosin phosphatase target subunit 1. *Gastroenterology* **144**, 1456-1465, 1465 e1451-1455 (2013).
52. Yamashiro, S., *et al.* Myosin phosphatase-targeting subunit 1 regulates mitosis by antagonizing polo-like kinase 1. *Dev Cell* **14**, 787-797 (2008).
53. Li, J., *et al.* Polo-like Kinase 1 Regulates Vimentin Phosphorylation at Ser-56 and Contraction in Smooth Muscle. *J Biol Chem* **291**, 23693-23703 (2016).
54. Gutteridge, R.E., Ndiaye, M.A., Liu, X. & Ahmad, N. Plk1 Inhibitors in Cancer Therapy: From Laboratory to Clinics. *Molecular cancer therapeutics* **15**, 1427-1435 (2016).
55. Olmos, D., *et al.* Phase I study of GSK461364, a specific and competitive Polo-like kinase 1 inhibitor, in patients with advanced solid malignancies. *Clin Cancer Res* **17**, 3420-3430 (2011).
56. Sebastian, M., *et al.* The efficacy and safety of BI 2536, a novel Plk-1 inhibitor, in patients with stage IIIB/IV non-small cell lung cancer who had relapsed after, or failed, chemotherapy: results from an open-label, randomized phase II clinical trial. *J Thorac Oncol* **5**, 1060-1067 (2010).
57. Hofheinz, R.D., *et al.* An open-label, phase I study of the polo-like kinase-1 inhibitor, BI 2536, in patients with advanced solid tumors. *Clin Cancer Res* **16**, 4666-4674 (2010).
58. Komrokji, R.S., *et al.* Phase I clinical trial of oral rigosertib in patients with myelodysplastic syndromes. *Br J Haematol* **162**, 517-524 (2013).
59. Vega, F.M. & Ridley, A.J. Rho GTPases in cancer cell biology. *FEBS Lett* **582**, 2093-2101 (2008).
60. Mardilovich, K., Olson, M.F. & Baugh, M. Targeting Rho GTPase signaling for cancer therapy. *Future Oncol* **8**, 165-177 (2012).

FIGURE LEGENDS

Figure 1. Genetic ablation of *Plk1* in adult mice. (**a**) Survival curve of 3-month-old mice of the indicated genotypes: *Plk1*(+/Δ); Cre-ERT, *Plk1*(Δ/Δ); Cre-ERT, and *Plk1*(lox/lox) (in the absence of the Cre allele) injected with three doses of tamoxifen (arrows). Log-rank Test (Mantel-Cox) ***, $p<0.001$. (**b**) Body weight of the mice shown in **a** (mean ± SD) . One-Way Anova; ***, $p<0.001$. (**c**) H&E staining of the intestinal mucosa in 10-week-old *Plk1*(Δ/Δ) and *Plk1*(lox/lox) control mice. The architecture is disrupted in *Plk1*(Δ/Δ) mice, where abnormal mitotic figures are observed (monopolar-like structures; arrows in the inset). Scale bars, 200 μm. Images are representative of 3 *Plk1*(lox/lox) and 8 *Plk1*(Δ/Δ) mice analyzed. (**d**) Left, immunohistochemical detection of phospho-Ser10 Histone H3 (pH3) and Plk1 in *Plk1*(lox/lox) (top row) and *Plk1*(Δ/Δ) (bottom row) mice. Scale bars, 50 μm. Top right, quantification of the percentage of pH3- and Plk1-positive cells (Columns indicate mean; $n>500$ cells from 3 mice per genotype). ***, $p<0.001$; 2-way ANOVA test. Bottom right, high magnification image of an aberrant mitotic (positive for pH3) cell that is negative for Plk1 staining. The dashed yellow line depicts the cell contour, and arrow heads indicate the spindle poles. Scale bar, 10 μm. (**e**) Survival curve of *Plk1*(+/–) mice [red; n=21; 11 females (blue) and 10 males (purple)] versus *Plk1*(+/+) controls (n=23) over 24 months. **, $p<0.01$; Log-rank Test (Mantel-Cox). (**f**) Orcein staining to highlight elastic fibers and H&E staining of the aorta of a *Plk1*(+/–) mouse, showing aortic rupture (open arrowhead, left micrograph) accompanied by fragmentation of elastic fibers (closed arrowheads, middle micrograph) and intramural hematoma (arrowheads, right micrograph). Scale bars, 200 μm (left) and 50 μm (middle and right). (**g**) Left, Van Gieson staining for elastin in aortic walls of 20-week-old *Plk1*(+/+) and

Plk1(+/–) mice. Scale bars, 50 μm. Right, quantification of the number of elastic fiber breaks per section (mean ± SD; n=3 sections from 4 [*Plk1*(+/–) AS and *Plk1*(+/+) DIA] or 5 (all other groups) mice. AS, ascending aorta; DIA, diaphragmatic abdominal aorta; SR, suprarenal abdominal aorta. (**h**) Left, representative ultrasound images of the aorta in 20-week-old *Plk1*(+/+) and *Plk1*(+/–) mice. Yellow dashed arrows indicate the aortic internal diameter. Scale bars, 1 mm. Right, quantification of the maximal aortic diameter (mean ± SD; n=7 wild-type and 5 heterozygous mice per group) of the indicated regions of the aorta. In (g, h), **, p<0.01; ***, p<0.001; Student's t-test.

Figure 2. Plk1 function in VSMCs *in vivo* (**a**) Representative analysis of *Plk1* alleles by PCR amplification. The presence of the lox and Δ alleles was determined in the aorta (A) and heart (H) of 10-week-old *Plk1*(lox/lox);SM22-Cre mice without tamoxifen (TAM) treatment [*Plk1*(lox/lox) genotype] or with TAM treatment [*Plk1*$(\Delta/\Delta)^{SM}$ genotype[. (**b**) *Plk1* mRNA levels (relative to *Gapdh* mRNA levels) in the indicated tissues from *Plk1*(lox/lox) and *Plk1*$(\Delta/\Delta)^{SM}$ mice. Columns indicate mean; n=3 mice per group; *, p<0.05; ns, not significant; Student's t-test. (**c**) Internal diameter of the ascending (AS), diaphragmatic (DIA) and suprarenal (SR) aorta scored by ultrasound measurements in 20-week-old *Plk1*(lox/lox) (n=9) and *Plk1*$(\Delta/\Delta)^{SM}$ (n=10) mice. *, p<0.05; Student t-test analysis. (**d**) Systolic blood pressure of *Plk1*$(\Delta/\Delta)^{SM}$ and *Plk1*(lox/lox) mice, as measured by a tail-cuff system (horizontal bars indicate mean). ***, p<0.001; Student t-test. (**e**) Analysis of the elasticity of aortic rings from *Plk1*$(\Delta/\Delta)^{SM}$ or *Plk1*(lox/lox) mice using a myograph (mean ± SEM). *, p<0.05; **, p<0.01; ***, p<0.001; Two-Way Anova analysis. (**f**) Contraction force in aortic rings from mice with the indicated genotypes in the presence of the indicated concentrations

of angiotensin II (Ang II) and phenylephrine (PE). Contraction is expressed as a percentage of the maximal KCl-induced contraction. Data are mean ± S.D.. (***, $p<0.0001$; Extra sum-of-squares F test). (**g**) Systolic blood pressure of *Plk1*$(\Delta/\Delta)^{SM}$ and *Plk1*(lox/lox) mice infused with AngII for the indicated amounts of time. The curves drawn represent the One-phase association nonlinear fit approximation (mean ± SEM; n=7 *Plk1(lox/lox)* and n=8 *Plk1*$(\Delta/\Delta)^{SM}$ mice). *, $p<0.05$; Student's t-test #, $p<0.05$; ##, $p<0.01$; Two-Way Anova analysis. (**h**) Heart weight normalized to tibia length in mice from panel **g** treated with AngII [*Plk1*(lox/lox) n=7; *Plk1*$(\Delta/\Delta)^{SM}$ n=8] or untreated [Ctrl; *Plk1*(lox/lox) n=18; *Plk1*$(\Delta/\Delta)^{SM}$ n=7] at the end of the experiment**, $p<0.01$; ***, $p<0.001$ Student's t-test. (**i**) Left ventricle (LV) septum and posterior wall thickness, as assessed by ultrasound, in mice from panel g treated with AngII [*Plk1*(lox/lox) n=7; *Plk1*$(\Delta/\Delta)^{SM}$ n=8] or untreated [Ctrl; *Plk1*(lox/lox) n=9; *Plk1*$(\Delta/\Delta)^{SM}$ n=10] at the end of the experiment. *, $p<0.05$; Student's t-test. (**j**) Quantification of cardiomyocyte area in mice from panel g treated with AngII or untreated (Ctrl) at the end of the experiment. The area of >500 cardiomyocytes per mouse (individual columns) were measured by staining with fluorescein isothiocyanate-conjugated wheat lectin. ***, $p<0.001$; One-way Anova. (**k**) Van Gieson staining of elastin (left; arrowheads indicate fiber breaks) and quantification of these breaks (right) in the wall of the ascending aorta of mice from panel g treated with AngII [*Plk1*(lox/lox) n=7; *Plk1*$(\Delta/\Delta)^{SM}$ n=7] or untreated [Ctrl; *Plk1*(lox/lox) n=6; *Plk1*$(\Delta/\Delta)^{SM}$ n=7] at the end of the experiment *, $p<0.05$; **, $p<0.01$; One-way Anova analysis. Scale bars, 50 μm.

Figure 3. Plk1 modulates the RhoA pathway in interphase VSMCs. (**a**) Schematic representation of the cellular protocol used for the analysis of interphase VSMCs. (**b**) F-actin staining to visualize cell morphology and actin stress fibers in *Plk1*(lox/lox) and *Plk1*(Δ/Δ) VSMCs 6 h after seeding in the presence of LPA (2 μM) as depicted by. Scale bars, 20 μm. (**c**) Cell roundness factor of *Plk1*(lox/lox) and *Plk1*(Δ/Δ) VSMCs that were plated in the presence or absence of 2 μM LPA and incubated for 2 or 6 hours after plating. Each circle represents a single cell and bars indicate the mean (n>50 cells per group in 3 different experiments). *, $p<0.05$; ***, $p<0.001$; One-Way Anova. (**d**) Top, immunoblotting for Plk1, phosphorylated Mypt1 (pMypt1 Thr696) and MLC (pMLC Ser18/19) after treatment of VSMCs of the indicated genotypes with 0.5 μM AngII for 5 min in Total Mypt1, MLC and α-tubulin were used as loading controls. Images are representative of three independent experiments. Bottom, representative images of the actin cytoskeleton (green) and MLC phosphorylation (red) in AngII-treated cells are shown. DAPI (blue) was used to stain the DNA. Scale bars, 20 μm. (**e**) Immunoblotting for active and total RhoA in pull-downs using the rhotekin-binding domain (RBD) as a bait from lysates of VSMCs of the indicated genotypes without or with LPA treatment for 5 min. A representative blot is shown from 3 different experiments. (**f**) Immunoblotting for active and total RhoA activity (RBD pull-downs) and pMLC after treatment of wild-type VSMCs without or with AngII and the indicated Plk1 inhibitors (GW, GW843682X; BI, BI2536). Total RhoA and α-tubulin were used as loading controls. (**g**) Cell roundness factor of wild-type VSMCs plated in the presence of 2 μM BI2536 (+) or DMSO (–). The cells were plated in the presence of 2 μM LPA and the cell roundness factor was measured 2 and 10 h after plating. Bars indicate mean (n>50 cells per group in 3 different experiments). **, $p<0.01$; One-Way

745 Anova. **(h)** Contraction force test in aortic rings isolated from 6-8-month old mice in
746 untreated (Control) or treated with DMSO or BI2536. The rings were stimulated with
747 increasing concentrations of angiotensin II (AngII; Control n=8; DMSO n=4; BI2536
748 n=4 mice) or phenylephrine (PE; Control n=6; DMSO n=6; BI2536 n=5 mice).
749 Contraction is expressed as a percentage of the maximal induced contraction reached in
750 the untreated samples. Data are mean ± S.D. ($p<0.0001$; Extra sum-of-squares F test).
751 (**i**) Representative images of phalloidin staining to visualize VSMC morphology and F-
752 actin staining in *Plk1*(lox/lox) VSMCs (top row) and *Plk1*(Δ/Δ) VSMCs (middle row)
753 transfected with either a control retrovirus (empty vector, EV) or a retrovirus expressing
754 the constitutively active RhoA-Q63L mutant. In addition, *Plk1*(lox/lox) cells that had
755 been transfected with EV or the RhoA-Q63L mutant were treated with the ROCK
756 inhibitor Y27632 (1 μM) (bottom row). Scale bars, 20 μm. (**j**) Cell roundness factor of
757 VSMCs from **i** 10 h after seeding. Bars indicate mean (n>50 cells per group in 3
758 different experiments). *, $p<0.05$; **, $p<0.01$, ***, $p<0.001$; One-Way Anova test.
759 Micrographs in (b,d,i) show representative images from 3 independent experiments.
760
761 **Figure 4.** Plk1 modulates activation of the RhoA pathway by Ect2. (**a**) Transcriptional
762 profiling of Ect2-, MyoGEF-, LARG-, p115GEF-, and RacGAP1-encoding transcripts
763 in aortas of wild-type mice treated with AngII for the indicated number of days.
764 Columns indicate mean; n=3 independent experiments; n.s., not significant; ***,
765 $p<0.001$; 2-Way ANOVA. (**b**) Cell roundness factor of VSMCs 2 and 10 h after plating
766 cells in the presence of 2 μM of LPA; the cells had been treated with scramble siRNAs
767 (Scr), or siRNAs targeting transcripts encoding Ect2, MyoGEF, LARG, p155GEF, or
768 RacGAP1. (**c**) Representative images of LPA-treated VSMCs transduced with Scr or

Ect2 or siRNA, 10 h after plating. Scale bars, 20 μm. (**d**) Cell roundness factor of wild-type VSMCs after treatment with AngII and the indicated siRNAs, or after treatment of *Plk1*(Δ/Δ) VSMCs with AngII for 10 h. (sh1 and sh2 correspond to two different shRNAs against Ect2) In **b** and **d**, bars indicate mean (n>50 cells per group in 3 different experiments). *, $p<0.05$; **, $p<0.01$; One-way ANOVA. (**e**) Immunoblotting for pMLC Ser19 in VSMCs treated as in **d.** The numbers indicate the relative level of phosphorylation in the presence of AngII versus scramble shRNA in the presence of AngII. α-tubulin was used as a loading control. (**f**) Left, immunoblotting for phospho-RacGAP1 (Ser170) (top arrow) and phospho-MLC (Ser19) (bottom arrow) in serum-starved VSMCs treated with 2 μM BI2536 or DMSO (Ctrl) and then stimulated with 2 μM LPA for 10 or 30 min. Total MLC and α-tubulin were used as loading controls. Right, quantification of the phospho-RacGAP1 and phospho-MLC levels, normalized to α-tubulin or total MLC, respectively in three independent experiments (columns indicate mean). (**g**) Immunoblotting for phospho-RacGAP1 (Ser170) (top arrow), phospho-MLC (Ser19) (bottom arrow) in serum-starved VSMCs treated with BI2536 or DMSO (Ctrl) and then stimulated with either 2 μM AngII (A) or 2 μM LPA (L) for 30 minutes. Total MLC was used as a loading control. Crtl samples were re-arranged from the same blot to correspond with BI2536-treated samples. (**h**) Immunoblotting for Ect2, wild-type GFP-RacGAP1 ($RacGAP1^{WT}$) or a mutant form of RacGAP1 with four phospho-mimetic mutations in the Plk1 phospho-sites ($RacGAP1^{4D}$) in pull down experiments using GST-RhoA-G17A in extracts from HEK293 cells expressing GFP-Ect2, GFP-$RacGAP1^{WT}$ or GFP-$RacGAP1^{4D}$, respectively. Cells were stimulated with 2 μM LPA for 20 min in the presence or absence of the Plk1 inhibitor BI2536. Data in (d,e,f) show representative images from 2 independent experiments.

Figure 5. Dynamic re-localization of Plk1 and Ect2 and its control by aPKC. **(a)** Immunofluorescent detection of endogenous Plk1 and phospho-MLC (pMLC) in untreated (NT, top) and AngII-treated (bottom) VSMCs, showing re-localization of Plk1 to the membrane edge upon AngII treatment, where Plk1 (red) co-localizes with phospho-MLC(Ser18/19) (green). Insets show single-channel images of the boxed regions**.** Actin fibers are visualized using phalloidin coupled to Alexa647 dye. DNA is counterstained with DAPI (blue). Scale bars, 10 μM (**b**) Time lapse images showing the localization of GFP-Ect2 to the cell edge and membrane protrusions (arrowheads) at the indicated time points after LPA treatment. Insets show higher magnification views of the boxed regions. The corresponding phase contrast images are also shown. Scale bar, 10 μM. (**c**) Immunoblotting for GFP-Ect2 or myc-Plk1 in HEK293 cells expressing GFP-Ect2 and myc-Plk1. The cells were treated with 2 μM LPA for the indicated time points with or without 1 μM PKC inhibitor Go6983. Top, cell lysates were subjected to myc-Plk1 immunoprecipitation (myc IP), and the immunoprecipitates were probed with anti-GFP or anti-myc antibodies. Numbers indicate the quantification of GFP-Ect2 band intensity in the IP versus input. Bottom, GFP-Ect2 and myc-Plk1 in the total cell extract (input). (**d**) Cell roundness factor of Plk1-null VSMCs (Δ/Δ) and wild-type cells (lox/lox) that were untreated or treated with either the ROCK inhibitor Y27632 (1 μM) or the PKC inhibitor Go6983 (1 μM). Mean ± SEM; n>50 cells per group in 3 different experiments. *, $p<0.05$; One-way ANOVA. (**e**) Top, immunoblotting for GFP-Ect2 and RhoA-G17A in pull-down experiments performed with GST-RhoA-G17A beads, using extracts from HEK293 cells, treated without or with LPA, expressing GFP-Ect2-WT, GFP-Ect2-T327A or GFP-Ect2-14A.RhoA-G17A was used as a control to show equal

loading of the coated beads. Numbers indicate the quantification of GFP-Ect2 band intensity in the IP versus input. Bottom, GFP-Ect2 in the total cell extracts (input). Lanes 1-4 and 5-6 were splitetd from the same blot membrane. (**f**) Top, immunoblotting for GFP-Ect2 in pull-down experiments performed with beads coated with GST-Plk1-PBD, using extracts of LPA-stimulated HEK293 cells expressing either wild-type (WT) GFP-Ect2 or the GFP-Ect2-T327A mutant. Numbers indicate the quantification of GFP-Ect2 band intensity in the IP versus input. Red Ponceau staining was used to monitor protein loading. Bottom, GFP-Ect2 in the total cell extracts (input). (**g**) Cell roundness factor of VSMCs treated with scramble shRNA (Scr) or two different shRNAs targeting mouse *Ect2* (sh1 and sh2). The cells were untransfected or expressed human wild-type Ect2 (WT) or the Ect2-T327A mutant. Data in (c,e,f) show representative blots from 2 independent experiments.

Figure 6. Plk1 inhibition impairs vascular homeostasis *in vivo*. (**a**) Experimental design. Twelve-week-old mice were injected twice per week with volasertib (15 mg/kg; n=13) or DMSO (n=11) for three weeks (red arrows). One week later, 8 mice from the volasertib group and 6 mice from the DMSO control group were treated with AngII (blue arrow) (**b**) Elasticity of aortic rings, as assessed using a myograph, from mice treated with DMSO (n=4 rings per mouse; 4 mice) or volasertib (n=4 rings per mouse; 4 mice) for two months. ***, $p<0.001$; Two-way Anova analysis. (**c**) Normalized blood pressure in DMSO treated mice (Ctrl), AngII, volasertib or the combination of AngII plus volasertib . Time 0 was immediately before AngII pump implantation. *, $p<0.05$; **, $p<0.01$; ***, $p<0.001$; Two Way-Anova. Red asterisks denote statistical significance between control+AngII treated mice and volasertib+AngII mice. Blue asterisks indicate statistical significance between control+AngII treated mice and non-

AngII treated animals. (**d**) Heart weight of mice from **c**, normalized to tibia length. DMSO-Control n=4; DMSO-AngII n=6; Volasertib-Control n=5; Volasertib-AngII n=6 mice; **, $p<0.01$; Student t-test. (**e**) Internal diameter of ascending (AS), diaphragmatic (DIA) and suprarenal (SR) aorta, as assessed by ultrasound, in 20-week-old mice from panel **c**. DMSO-Control n=5; DMSO-AngII n=6; Volasertib-Control n=5; Volasertib-AngII n=8 mice; *, $p<0.05$; **, $p<0.01$; Student t-test analysis. (**f**) Van Gieson staining for elastin. Left, quantification of elastic breaks in the ascending [DMSO-Control n=5; DMSO-AngII n=6; Volasertib-Control n=4; Volasertib-AngII n=8 mice] and abdominal [DMSO-Control n=5; DMSO-AngII n=6; Volasertib-Control n=5; Volasertib-AngII n=8 mice] aortic walls from mice in panel **c**. Right, representative images of the abdominal aorta from the groups of mice indicated in panel a. *, $p<0.05$; **, $p<0.01$; ***, $p<0.001$. Student t-test analysis. Scale bars, 100 μm. (**g**) Representative macroscopic (top) and microscopic images of the abdominal aorta of 20-week-old mice treated with AngII and DMSO or volasertib, showing the presence of aortic aneurysm and aortic wall rupture in AngII plus volasertib treated mice. Hematoxylin and Eosin (H&E) staining (second and third rows) and elastin Van Gieson staining (EVG, bottom row) are shown. Arrowheads indicate rupture of the aorta wall. Histology images are representative of the three aortas per group in the upper panel. Scale bars, 0.5 mm (top H&E row); 100 μm (bottom H&E and EVG rows).

ON-LINE METHODS

Mice. The *Plk1*(lox) and *Plk1*(–) alleles were recently described[13,14]. For whole-body conditional ablation of *Plk1*, we used the RERT2 allele, which carries a tamoxifen-inducible Cre recombinase ubiquitously expressed under the regulatory sequences of RNA polymerase II[15]. Mice (*Mus musculus*) were maintained in a mixed 129/Sv x C57BL/6J background and both males and females were indistinctly used unless otherwise specified. Wild-type female mice in the volasertib experiments were pure C57BL/6J background. *Plk1*(+/lox) and *Plk1*(lox/lox) mice were used to generate *Plk1*(+/Δ) and *Plk1*(Δ/Δ) mice, respectively, after i.p. injection with tamoxifen citrate salt (0.1 mg/g of animal weight). Quantitative analysis of blood cell populations was performed in 10-20-week-old mice using a veterinary hematology analyzer Procount (Ser nr. 901235) using K3-EDTA 3K (Aquisel #1501126) as an anticoagulant. For specific ablation of Plk1 in VSMCs, we used the SM22-Cre model reported previously[17]. 10-week-old mice were fed ad libitum with a tamoxifen-supplemented diet (Harlan Laboratories Models) and analyzed after 8-12 weeks of treatment. For AngII perfusion, subcutaneous micro-osmotic pumps (Alzet) were used. AngII (Sigma) was diluted in saline buffer and loaded into these osmotic pumps to obtain a delivery ratio of 0.5 μg/kg/min over the course of two (Alzet 1002) or four weeks (Alzet 1004). For volasertib treatment, 3-month-old mice were intravenously injected with either 15 mg/kg BI6727 (Selleckchem) as reported previously[61] or with 1% DMSO in saline buffer as a control, twice per week following the scheme represented in Fig. S6a. GW843682X (Selleckchem) was injected at 8.5 mg/kg intraperitoneally every 4 days for 2 weeks. Sample sizes were estimated based on previously published experiments and mice were not randomized. The investigators were not blinded to experimental

887 group in outcome assessment. Mice were housed at the pathogen-free animal facility of
888 the Centro Nacional de Investigaciones Oncológicas (CNIO, Madrid) following the
889 animal care standards of the institution. These animals were observed on a daily basis
890 from birth to death and sick mice were euthanized humanely in accordance with the
891 Guidelines for Humane End Points for Animals used in biomedical research.
892
893 **Anatomical, cytological and histological analysis.** Heart weight was measured after
894 heart dissection and cleaning of the surrounding fat tissue. Heart weight (mg) was then
895 normalized versus the tibia length (mm) for each animal. Heart left ventricle septum and
896 posterior wall thickness were measured either in post-mortem histological heart
897 sections, or *in vivo* by echocardiography (Vevo 2100 ecography device, VisualSonics,
898 Toronto). For histological observation, dissected organs were fixed in 10%-buffered
899 formalin (Sigma) and embedded in paraffin wax. Three- or five-micrometer-thick
900 sections were stained with hematoxylin and eosin (H&E), Orcein, or Elastin Van
901 Gieson's (EVG) for elastic fiber detection, fluorescein isothiocyanate-conjugated wheat
902 lectin (FITC-WGA) for measuring cardiomyocyte size, and Alcian Blue to detect
903 mucopolysacharide deposition. Elastic fiber breaks were quantified using at least three
904 different sections of the same aortic region in all treated animals. Similarly,
905 cardiomyocyte area was quantified from three different heart sections in each sample
906 from all treated animals. Additional immunohistochemical examination of tissue was
907 performed using specific antibodies against Ki67 (Master Diagnostica), phospho-
908 histone H3 Ser10 (Millipore 06-570), or a new monoclonal antibody generated against
909 human Plk1[13,14].
910 For transmission electron microscopy, aortas were dissected and sliced into
911 small fragments of 3 mm to 5 mm each. Aorta slices were then fixed in a mixture of

912 1.25% glutaraldehyde + 2.5% paraformaldehyde in PBS for 2 hours, and subsequently
913 in a 2% osmium tetroxide solution. Fixed aortas were then embedded in Lowicryl
914 plastic resin (Polyscience, Warrington – PA) following the manufacturer's instructions.
915 Ultrathin cuts of 60 nm were mounted in formvar coated nickel grids and examined
916 using a JEOL JEM-100CX transmission electron microscope at 60kV voltage.
917
918 **Arterial contractility and elasticity.** Thoracic aortas or mesenteric arteries were
919 removed from 30-week-old mice, and placed in chilled Krebs solution containing 118
920 mM NaCl; 4.7 mM KCl; 2.5 mM $CaCl_2$; 1.2 mM KH_2PO_4; 1.2 mM $MgSO_4$; 25 mM
921 $NaHCO_3$; and 11 mM glucose. The pH of the solution after saturation with carbogen
922 (95% O_2 and 5% CO_2 mixture) was 7.4. The aorta and first or second branch mesenteric
923 arteries were carefully cleaned of fat and connective tissue and cut into rings (2 mm in
924 length). Aortic rings were mounted between two steel wires (40 μm diameter)
925 introduced through the lumen, onto a four channel wire myograph (DMT A/S,
926 Denmark). Similarly mesenteric arteries were mounted between two tungsten wires (25
927 μm). After an equilibration period of 20 minutes, all rings were normalized to a pressure
928 equal to 90 mmHg. Aortic rings were set at a resting tension of 5 mN and allowed to
929 equilibrate for 30 min. At the end of the equilibration period, the vessels were tested for
930 responsiveness a hyperpotassium solution (KPSS, KCl 120 mM) and washed with
931 Krebs solution. After that, cumulative concentration-response curves to phenylephrine
932 (10^{-9}-10^{-4} M) or angiotensin II (10^{-10}-10^{-6} M) were performed in separate rings until the
933 maximal response was consistent. Vasoconstrictor responses were expressed as a
934 percentage of KCl-induced contractions. In some rings, after a period of washing and
935 stabilization new concentration-response curves were repeated after 30-min incubation
936 with either DMSO as solvent, BI2536, GO6983 or Y27632. Data were expressed as a

937 percentage of the maximal response to the agonist in the absence of the antagonist. In
938 another series of experiments, aortic rings elasticity was tested 15 minutes after
939 normalization process, by forcing the aortic rings to a progressive stretching from the
940 basal level to a 150 μm distance, in steps of 10 μm every 50 sec, and measuring the
941 tension reached in each step. The cumulative concentration-response curves, with and
942 without the antagonists, were fitted to a logistic equation and analyzed using GradPad
943 Prism 5.0 software. Each point indicates the mean ± standard error of the mean
944 (S.E.M.). To compare concentration–response curves, statistical analysis was performed
945 using the extra sum-of-squares F test principle.
946
947 **Blood pressure measurements and *in vivo* imaging.** Mice arterial blood pressure was
948 measured with an automated tail-cuff BP-2000 Blood Pressure Analysis System
949 (Visitech Systems, Apex, NC, USA). In brief, mice were trained for BP measurements
950 conditions for one week on a daily basis. After training, the BP was measured twice
951 before implantation of angiotensin II (AngII) pumps, to determine the basal blood
952 pressure values in each mice cohort. Blood pressure measurements were performed by
953 placing mice in tail-cuff restrainers over a warmed surface (39 ºC)**.** Fifteen consecutive
954 systolic blood pressure measurements were done, and the last ten readings per mouse
955 were recorded and averaged.
956 Ascending and descending aortic diameter was monitored in isofluorane-
957 anaesthetized mice by the high-frequency ultrasound Vevo 2100 echography device
958 (VisualSonics, Toronto). Images were taken at three levels of the aorta: ascending (AS),
959 diaphragmatic abdominal (DIA) and suprarenal abdominal (SR) aorta. Maximal internal
960 diameters of aortic images were measured using VEVO 2100 version 1.5.0 software.
961

RNA analysis. For microarray expression analysis, total RNA was extracted from aortas of mice at the age of 3-5 months, using Trizol reagent as indicated in manufacturer´s instructions (Invitrogen). The quality of obtained RNA was evaluated using the Lab-Chip technique (Agilent Bioanalyzer). Samples were then fluorescently labeled by *in vitro* transcription following the Two-Color Microarray-Based Gene Expression Analysis protocol (Quick Amp Labeling Kit, Two-Color; Agilent p/n 5190-0444). We used the Whole Mouse Genome Oligo Microarray (Agilent) containing 44,000 probes (60mers) that correspond to 41,000 different transcripts, as verified and optimized by the manufacturer. The images were acquired and quantified by means of a confocal scanner and software (Agilent G2565BA and Feature Extraction). The expression levels were processed using standard methods of normalization, FDR (false discovery rate) determination, and pathway analysis (GeneSpring, Ingenuity Pathway Analysis).

For single gene qRT-PCR analysis, RNA from mice aortas treated with AngII was extracted using Trizol and subsequently column-purified with the Absolutely RNA Miniprep Kit (Stratagene). Both cDNA synthesis and PCR amplification was performed using the SuperScript III One-Step RT-PCR System with Platinum® Taq DNA Polymerase (Invitrogen). Oligonucleotides used are listed in Supplementary Table 4. The amounts of mRNA were measured using SYBR Green, and amplification of the housekeeping gene GAPDH was used as a normalization control. All amplicons were analyzed using BioRad iQ5 Optical System Software (version 2.0.148.60623; BioRad; 170-9753SE01).

Cell culture, infection and transfection. Cells were grown in DMEM supplemented with 10% FBS, 1% pen/strep, and 1% L-glutamine. VSMCs were obtained following

the protocol described in ref. [62]. Briefly, the aorta was dissected out from its origin at the left ventricle to the iliac bifurcation and washed thoroughly in cold PBS. We removed adventitia from the aorta using angled forceps, as viewed using a dissecting microscope. Aortas were then sliced into ~1–2 mm pieces and these were incubated for 20 to 60 minutes in collagenase media [DMEM + 1% pen/strep + 1% L-glutamine + 0.04% w/v collagenase type II (C6885 Sigma)]. Collagenase was inactivated by adding 1 volume of DMEM + 10% FBS and the tissue was cleaned by repeated centrifugation and suspension in regular DMEM + 10% FBS. Aorta slices were then placed into tissue culture plates containing DMEM + 10% FBS and incubated for 2 days at 37 ºC. Once VSMC started to proliferate and attach to the plate, cells were trypsinized and expanded. Finally, VSMC were immortalized using the T121 construct that encodes the first 121 amino acids of the SV40 large T antigen[63]. Plk1 depletion was achieved by infecting serum starved *Plk1*(lox/lox) VSMCs with AdenoCRE viral particles (Ad5CMVCre supplied by University of Iowa Viral Vector Core Facility; Ref. #VVC-U). for 48 to 60 h. Transfection of siRNAs was done using the NEON nucleofection system (Invitrogen). Expression of wild-type and T327A human Ect2 cDNAs was achieved by lentiviral particle infection. Depletion of murine *Ect2* [Sigma Mission shRNAs TRCN0000190489 (sh1) and TRCN0000336440 (sh2)], *Racgap1* (Sigma Mission shRNA TRCN0000322156) or *Arhgef12* (encoding LARG; Sigma Mission shRNA TRCN0000109960) was performed by expressing lentiviral particles carrying shRNAs against the indicated transcripts. We also used commercial siRNAs (Dharmacon On-target pools) targeting *Ect2* (LQ-047092), *Arhgef12* (LQ-041056-01), *Arhgef1* (p115GEF; LQ-047092), *Plekhg6* (MyoGEF; LQ-056082-01) or *Racgap1* (LQ-041056-01).

Immunofluorescence and morphological analysis in cultured cells. Cell morphology analysis was done on VSMCs infected with AdenoCre viral particles, and/or nucleofected with the indicated siRNAs or shRNAs; treated with inhibitors of Plk1 (2 μM BI2536), aPKC (1 μM Go6983) or ROCK (1 μM Y27632); or transduced with a retroviral construct encoding the RhoA-Q63L constitutive active mutant[64] or lentiviral vectors expressing different human Ect2 cDNAs (Ref. [39]). Cells were then trypsinized and kept in suspension for 1 to 2 h in media without serum, to completely inhibit the RhoA pathway[65]. Cells were then plated on gelatin coated coverslips in the presence or absence of 2 μM lysophosphatidic acid (LPA) or 0.5 μM AngII, fixed in 4% formaldehyde in PBS for 15 minutes and permeabilized with 0.5% Triton X-100 and 0.1% SDS in PBS for 10 minutes. Cells were then stained with antibodies against phospho-MLC (Ser19; Cell Signaling #3675; 1:1000), or Plk1 (rat monoclonal clone POE125; 1:200; Ref. [14]); phalloidin coupled to a fluorescent dye (Molecular Probes) for actin detection; and DAPI for DNA counterstaining. Cell images were captured at low magnification (10x objective) with a Leica DMI6000 fluorescent microscope. Roundness data were obtained by applying the formula $(4 \cdot \text{Area})/(\pi \cdot (\text{major axis})^2)$, using the morphology analysis tools available in ImageJ software. Roundness numbers range from 0 to 1, where 1 indicates a perfectly round cell, and data below 1 indicates elongated or polygonal cells. Similar quantification of the roundness or elliptic morphology of mesenchymal cells has been previously used to describe these morphological changes and their dependence on RhoA activity[66].

Protein extraction and immunoblotting. Cells were washed twice with ice-cold TBS (150 mM NaCl; 50 mM TRIS/HCl; pH 7.5) and lysed in RIPA lysis buffer (37 mM NaCl, 0.5% NP-40, 0.1% SDS, 1% TX-100, 20 mM Tris-HCl pH 7.4, 2 mM EDTA,

10% glycerol, supplemented with protease and phosphatase inhibitory cocktails (SIGMA). After 30 min on ice, samples were vortexed (5 min at 4 ^{o}C) and cleared by centrifugation. Proteins were separated on XT Criterion Bis-Tris acrylamide gels (BioRad), transferred to nitrocellulose membranes (BioRad), and probed using the following specific antibodies: anti-phospho-RacGAP1 (Ser170; Active Motive #39265-66; 1:500); anti-phospho-MLC (Ser18/Ser19; Cell Signaling #3674; 1:1000)); anti-MLC (Cell Signaling #3672; 1:2000); anti-Plk1 (clone PL6/PL2; ThermoFIsher #33-1700; 1:500), anti-phospho-Mypt1-Thr696 (Cell Signaling #5163; 1:100); anti-Mypt1 (Santa Cruz Biotechnologies #sc-25618; 1:500) and anti-α-Tubulin (SIGMA, clone DM1A; #T9026; 1:10000). Signal detection was done using secondary antibodies coupled to Alexa 680 dye (Invitrogen) and using the Odyssey Infrared Imaging System (Li-Cor Biosciences).

GST pull downs. GST-RBD (Addgene; #15247) or GST-RhoA-G17A (obtained from Channing J. Der, University of North Carolina; Ref. [67]) recombinant beads were prepared as described in Refs. [68,69]. Pull downs were performed in HEK293 cell lysates expressing different GEF cDNA constructs. HEK293 cells were transfected with plasmids encoding GFP-ECT2 [39], GFP-LARG [70], GFP-p115GEF [70], GFP-RacGAP1 [26] and (3x)myc-Plk1 [71]. After cDNA expression for 24 h, cells were incubated in RPMI media without serum for 4 to 5 h and then induced with 2 μM LPA (SIGMA) for the indicated times. For Plk1 or PKC inhibition, 2 μM of BI2536 (JS Research Chemicals Trading, Germany) or 1 μM of Go6983 (Calbiochem) was added 1 to 2 h before LPA addition. Cells were then washed in cold TBS, and then cold-lysed either in RBD lysis buffer (50 mM TRIC/HCl, pH7.2; 500 mM NaCl, 10 mM $MgCl_2$; 1% TX100; 0.5%

sodium deoxycholate; and 0.1% SDS) or RhoA-G17A lysis buffer (50 mM Tris-HCl, pH7.4; 15 0mM NaCl; 5mM $MgCl_2$; and 1% TX100) supplemented with 0.5 mM DTT, protease inhibitor cockatil (Roche), and phosphatase inhibitor cocktail (Calbiochem). Lysates were immediately frozen in dry ice and stored at -80 ºC. Pull downs were done by adding either GST-RBD or GST-RhoA-G17A beads to 0.5 mg of total protein cell lysates. Beads were incubated in a rocking wheel at 4 ºC for 1 hour and then washed three times in the appropriate lysis buffer. Finally, beads were drained in loading buffer and proteins were separated on XT Criterion Bis-Tris acrylamide gels (BioRad), transferred to nitrocellulose membranes (BioRad), and probed using the following specific antibodies: anti-RhoA/B/C (Millipore clone 55, #05-778; 1:1000).; anti-GFP (Roche, clones 7.1/13.1; #1 814 460; dilution 1:1000); anti-Plk1 (ThermoFIsher clone PL6/PL2 #33-1700; 1:500) and anti-myc tag (Santa Cruz Biotechnologies, clone 9E10, #sc-40; 1:1000).).

Plk1-PBD (residues 326-608) fused to GST (a generous gift from Michael Yaffe; Ref. [25]) was expressed in bacteria and coupled to glutathione-sepharose beads (GE Healthcare). Plk1-PBD pull down assays were done similarly to the GST-RBD pull down assays.

Statistical analysis. Statistical analysis was performed using ANOVA analysis, two-sided Student's t-test or Chi-square (Log-rank Mantel-Cox) tests or extra sum-of-squares F test principle. All data are shown as mean with standard deviation (SD) or standard error of the mean (SEM). Probabilities of $p < 0.05$ were considered significant. Detailed information on experimental design and reagents can be found in the Life Sciences Reporting Summary.

REFERENCES TO METHODS

61. Rudolph, D., *et al.* BI 6727, a Polo-like kinase inhibitor with improved pharmacokinetic profile and broad antitumor activity. *Clin Cancer Res* **15**, 3094-3102 (2009).
62. Ray, J.L., Leach, R., Herbert, J.M. & Benson, M. Isolation of vascular smooth muscle cells from a single murine aorta. *Methods Cell Sci* **23**, 185-188 (2001).
63. Jat, P.S., *et al.* Direct derivation of conditionally immortal cell lines from an H-2Kb-tsA58 transgenic mouse. *Proc Natl Acad Sci U S A* **88**, 5096-5100 (1991).
64. Caloca, M.J., Zugaza, J.L., Matallanas, D., Crespo, P. & Bustelo, X.R. Vav mediates Ras stimulation by direct activation of the GDP/GTP exchange factor Ras GRP1. *EMBO J* **22**, 3326-3336 (2003).
65. Ren, X.D., *et al.* Disruption of Rho signal transduction upon cell detachment. *J Cell Sci* **117**, 3511-3518 (2004).
66. Grande-Garcia, A., *et al.* Caveolin-1 regulates cell polarization and directional migration through Src kinase and Rho GTPases. *J Cell Biol* **177**, 683-694 (2007).
67. Ren, X.D., Kiosses, W.B. & Schwartz, M.A. Regulation of the small GTP-binding protein Rho by cell adhesion and the cytoskeleton. *EMBO J* **18**, 578-585 (1999).
68. Waheed, F., Speight, P., Dan, Q., Garcia-Mata, R. & Szaszi, K. Affinity precipitation of active Rho-GEFs using a GST-tagged mutant Rho protein (GST-RhoA(G17A)) from epithelial cell lysates. *J Vis Exp* (2012).
69. Dubash, A.D., *et al.* A novel role for Lsc/p115 RhoGEF and LARG in regulating RhoA activity downstream of adhesion to fibronectin. *J Cell Sci* **120**, 3989-3998 (2007).
70. Reuther, G.W., *et al.* Leukemia-associated Rho guanine nucleotide exchange factor, a Dbl family protein found mutated in leukemia, causes transformation by activation of RhoA. *J Biol Chem* **276**, 27145-27151 (2001).
71. de Carcer, G., *et al.* Plk5, a polo box domain-only protein with specific roles in neuron differentiation and glioblastoma suppression. *Mol Cell Biol* **31**, 1225-1239 (2011).

EDITORIAL SUMMARY

Although Plk1 has been studied primarily as a mitotic regulator in dividing cells, de Cárcer *et al.* find that Plk1 deficiency or inhibition in mice leads to vascular defects, including aortic aneurysm and rupture, as well as defective vascular smooth muscle contractility. These results provide a note of caution to the clinical use of Plk1 inhibitors as anti-cancer agents.

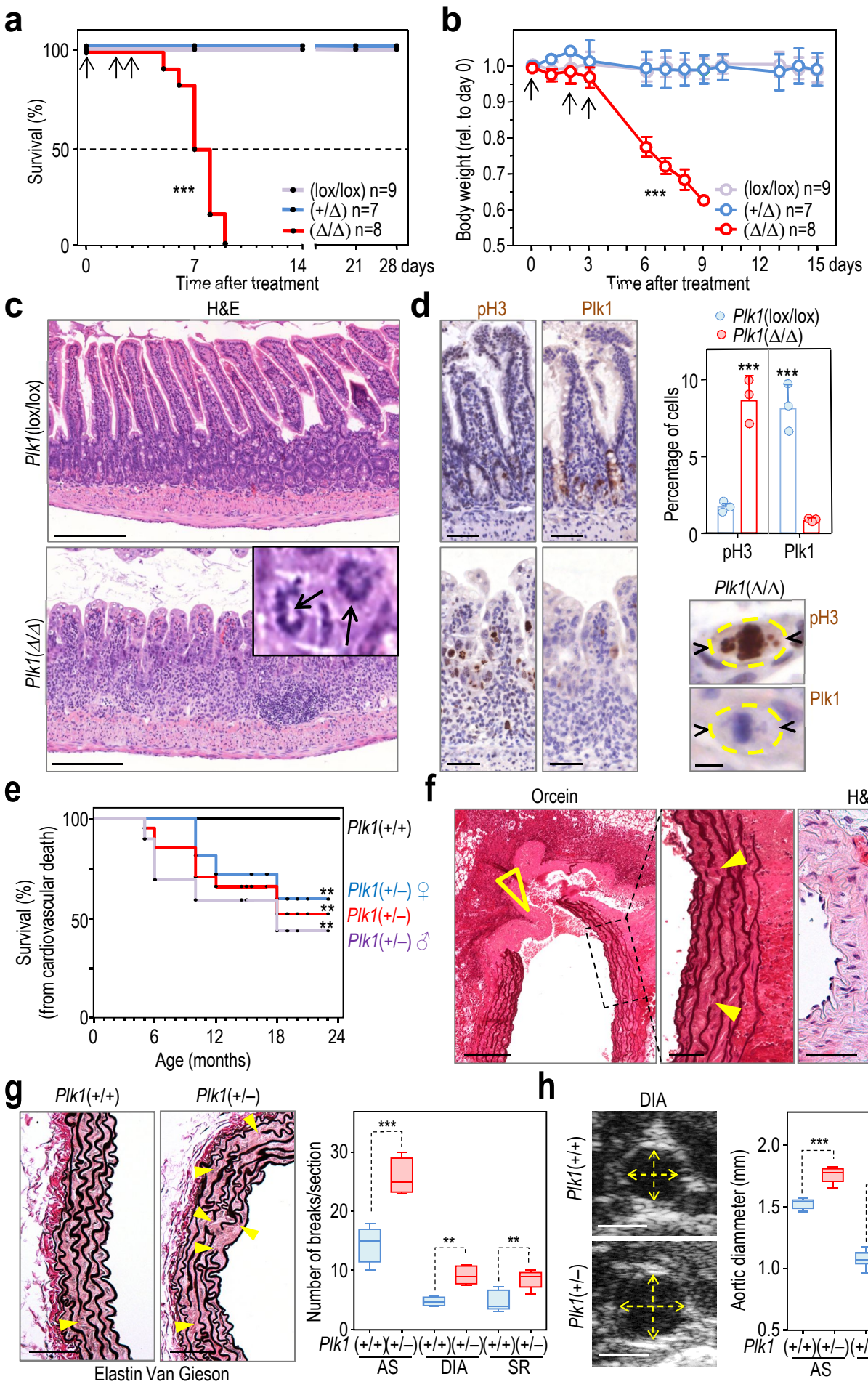
a
Survival (%)
100
50
0
***
(lox/lox) n=9
(+/Δ) n=7
(Δ/Δ) n=8
0
7
14
21
28 days
Time after treatment
b
Body weight (rel. to day 0)
1.0
0.9
0.8
0.7
0.6
0.5
***
(lox/lox) n=9
(+/Δ) n=7
(Δ/Δ) n=8
0
3
6
9
12
15 days
Time after treatment
c
H&E
Plk1(lox/lox)
Plk1(Δ/Δ)
d
pH3
Plk1
Plk1(lox/lox)
Plk1(Δ/Δ)
Percentage of cells
10
5
0
***
***
pH3
Plk1
Plk1(Δ/Δ)
pH3
Plk1
e
Survival (%)
(from cardiovascular death)
100
50
0
Plk1(+/+)
Plk1(+/–) ♀
Plk1(+/–)
Plk1(+/–) ♂
**
**
**
0
6
12
18
24
Age (months)
f
Orcein
H&E
g
Plk1(+/+)
Plk1(+/–)
Elastin Van Gieson
Number of breaks/section
30
20
10
0
***
**
**
Plk1 (+/+)(+/–)(+/+)(+/–)(+/+)(+/–)
AS
DIA
SR
h
DIA
Plk1(+/+)
Plk1(+/–)
Aortic diammeter (mm)
2.0
1.5
1.0
0.5
***
***
***
Plk1 (+/+)(+/–)(+/+)(+/–)(+/+)(+/–)
AS
DIA
SR

Figure 1

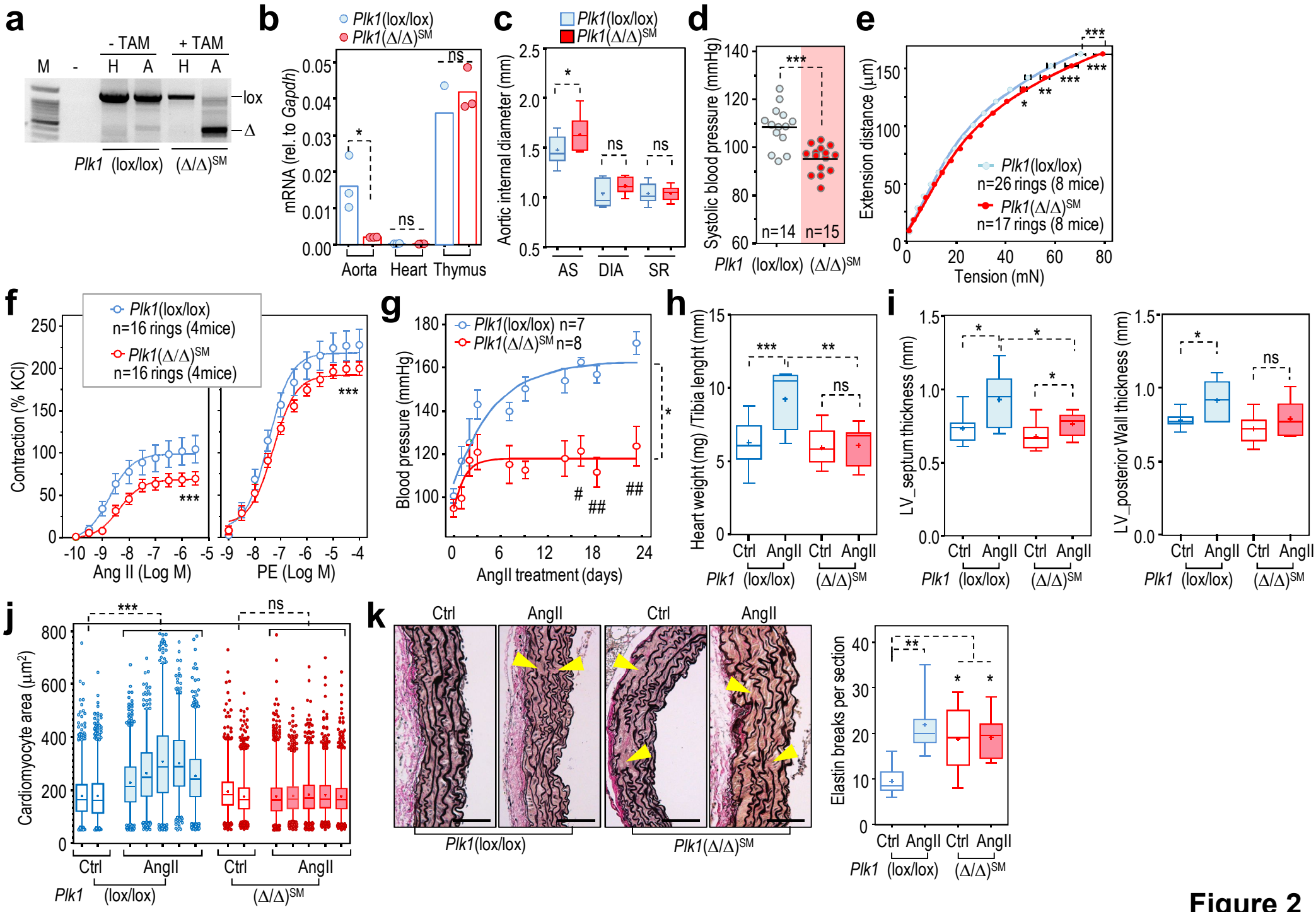
a
M
-
- TAM
+ TAM
H
A
H
A
lox
Δ
Plk1 (lox/lox) (Δ/Δ)SM
b
Plk1(lox/lox)
Plk1(Δ/Δ)SM
mRNA (rel. to Gapdh)
Aorta
Heart
Thymus
c
Aortic internal diameter (mm)
AS
DIA
SR
d
Systolic blood pressure (mmHg)
n=14
n=15
e
Extension distance (µm)
Tension (mN)
Plk1(lox/lox)
n=26 rings (8 mice)
Plk1(Δ/Δ)SM
n=17 rings (8 mice)
f
Plk1(lox/lox)
n=16 rings (4mice)
Plk1(Δ/Δ)SM
n=16 rings (4mice)
Contraction (% KCl)
Ang II (Log M)
PE (Log M)
g
Plk1(lox/lox) n=7
Plk1(Δ/Δ)SM n=8
Blood pressure (mmHg)
AngII treatment (days)
h
Heart weight (mg) /Tibia lenght (mm)
i
LV_septum thickness (mm)
LV_posterior Wall thickness (mm)
Ctrl
AngII
Plk1 (lox/lox) (Δ/Δ)SM
j
Cardiomyocyte area (µm2)
k
Ctrl
AngII
Plk1(lox/lox)
Plk1(Δ/Δ)SM
Elastin breaks per section

Figure 2

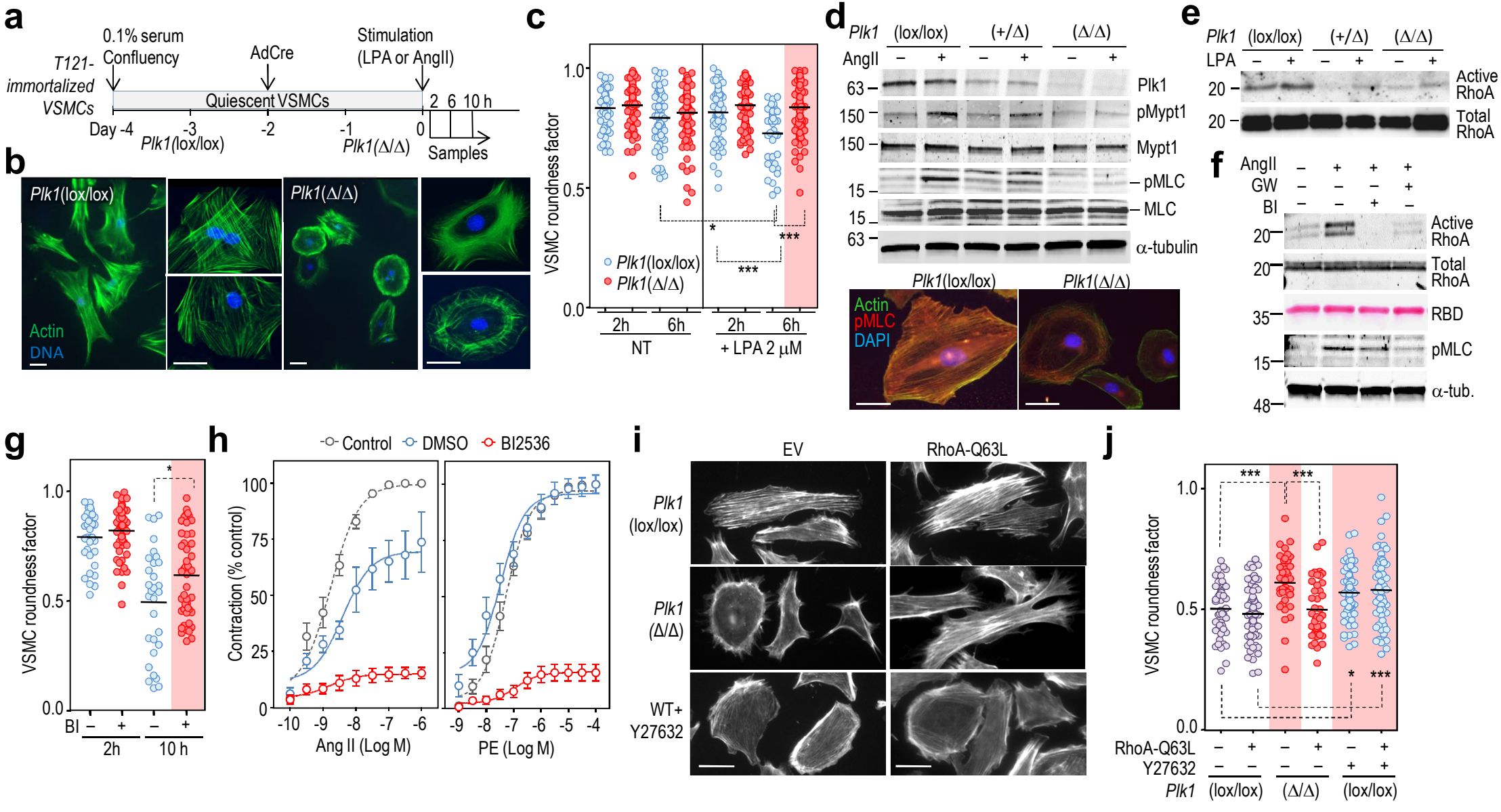
a
0.1% serum
Confluency
AdCre
Stimulation
(LPA or AngII)
T121-immortalized VSMCs
Quiescent VSMCs
2 6 10 h
Day -4
-3
-2
-1
0
Plk1(lox/lox)
Plk1(Δ/Δ)
Samples
b
Plk1(lox/lox)
Plk1(Δ/Δ)
Actin
DNA
c
VSMC roundness factor
1.0
0.5
0.0
Plk1(lox/lox)
Plk1(Δ/Δ)
*
***
***
2h
6h
2h
6h
NT
+ LPA 2 μM
d
Plk1 (lox/lox) (+/Δ) (Δ/Δ)
AngII – + – + – +
63
Plk1
150
pMypt1
150
Mypt1
15
pMLC
15
MLC
63
α-tubulin
Plk1(lox/lox)
Plk1(Δ/Δ)
Actin
pMLC
DAPI
e
Plk1 (lox/lox) (+/Δ) (Δ/Δ)
LPA – + – + – +
20
Active RhoA
20
Total RhoA
f
AngII – + + +
GW – – – +
BI – – + –
20
Active RhoA
20
Total RhoA
35
RBD
15
pMLC
48
α-tub.
g
VSMC roundness factor
1.0
0.5
0.0
*
BI – + – +
2h
10 h
h
Control
DMSO
BI2536
Contraction (% control)
100
75
50
25
0
-10 -9 -8 -7 -6
Ang II (Log M)
-9 -8 -7 -6 -5 -4
PE (Log M)
i
EV
RhoA-Q63L
Plk1 (lox/lox)
Plk1 (Δ/Δ)
WT+ Y27632
j
VSMC roundness factor
1.0
0.5
0.0
***
***
*
***
RhoA-Q63L – + – + – +
Y27632 – – – – + +
Plk1 (lox/lox) (Δ/Δ) (lox/lox)

Figure 3

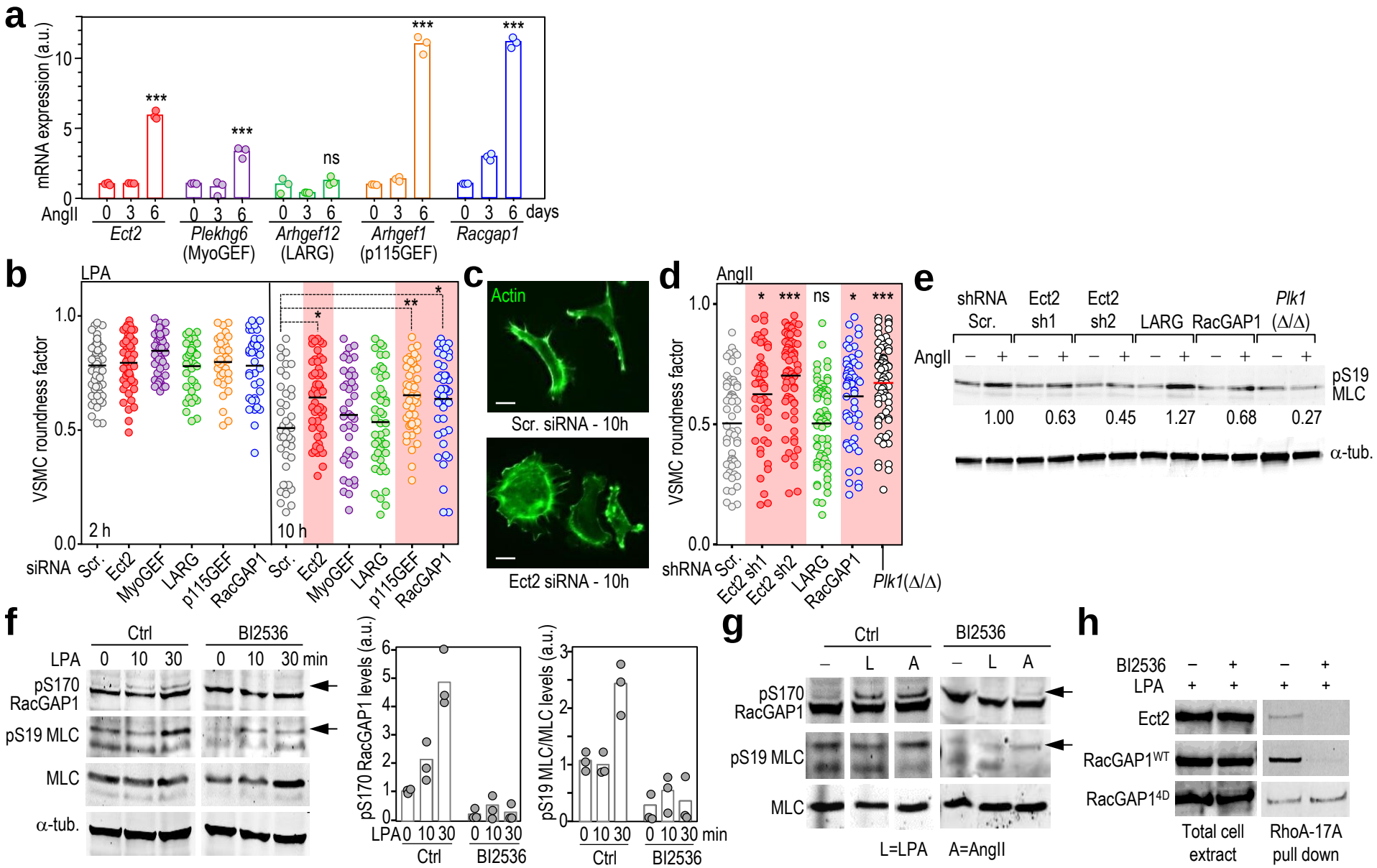
a
mRNA expression (a.u.)
AngII
0 3 6 days
Ect2
Plekhg6 (MyoGEF)
Arhgef12 (LARG)
Arhgef1 (p115GEF)
Racgap1
***
ns
b
LPA
VSMC roundness factor
2 h
10 h
siRNA Scr. Ect2 MyoGEF LARG p115GEF RacGAP1
c
Actin
Scr. siRNA - 10h
Ect2 siRNA - 10h
d
AngII
shRNA Scr. Ect2 sh1 Ect2 sh2 LARG RacGAP1 Plk1(Δ/Δ)
e
shRNA Scr. Ect2 sh1 Ect2 sh2 LARG RacGAP1 Plk1 (Δ/Δ)
AngII
pS19 MLC
1.00 0.63 0.45 1.27 0.68 0.27
α-tub.
f
Ctrl BI2536
LPA 0 10 30 0 10 30 min
pS170 RacGAP1
pS19 MLC
MLC
α-tub.
pS170 RacGAP1 levels (a.u.)
pS19 MLC/MLC levels (a.u.)
g
Ctrl BI2536
– L A – L A
pS170 RacGAP1
pS19 MLC
MLC
L=LPA A=AngII
h
BI2536 – + – +
LPA + + + +
Ect2
RacGAP1WT
RacGAP14D
Total cell extract
RhoA-17A pull down

Figure 4

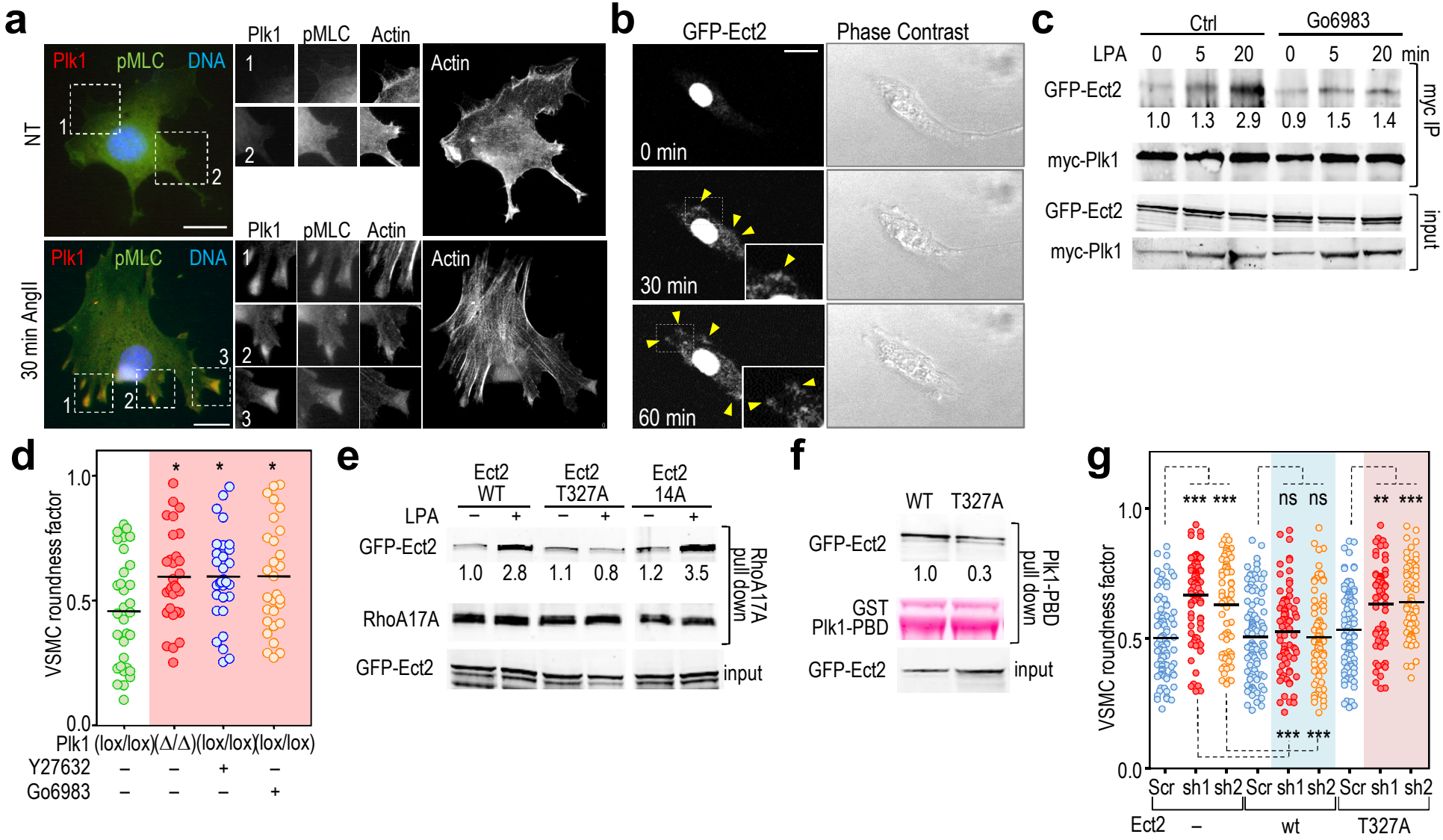
a
Plk1
pMLC
DNA
Actin
NT
30 min AngII
b
GFP-Ect2
Phase Contrast
0 min
30 min
60 min
c
Ctrl
Go6983
LPA
0
5
20
min
GFP-Ect2
myc-Plk1
1.0
1.3
2.9
0.9
1.5
1.4
myc IP
input
d
VSMC roundness factor
Plk1 (lox/lox)(Δ/Δ)(lox/lox)(lox/lox)
Y27632
Go6983
e
Ect2 WT
Ect2 T327A
Ect2 14A
RhoA17A
1.0
2.8
1.1
0.8
1.2
3.5
RhoA17A pull down
input
f
WT
T327A
GST Plk1-PBD
1.0
0.3
Plk1-PBD pull down
g
ns
Scr
sh1
sh2
Ect2
wt
T327A

Figure 5

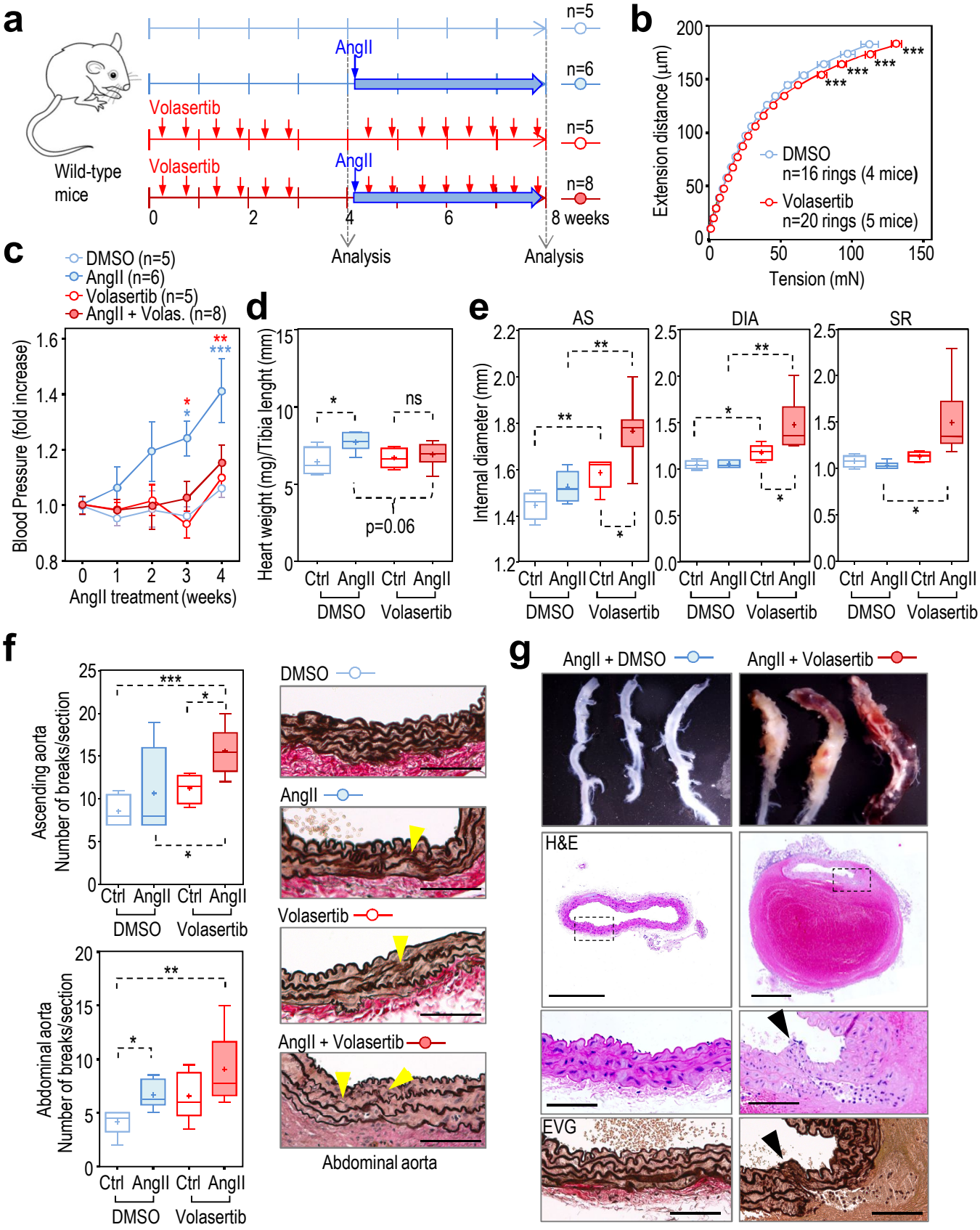
a
Wild-type mice
AngII
Volasertib
Volasertib
AngII
n=5
n=6
n=5
n=8
0
2
4
6
8 weeks
Analysis
Analysis
b
Extension distance (µm)
Tension (mN)
DMSO
n=16 rings (4 mice)
Volasertib
n=20 rings (5 mice)
c
DMSO (n=5)
AngII (n=6)
Volasertib (n=5)
AngII + Volas. (n=8)
Blood Pressure (fold increase)
AngII treatment (weeks)
d
Heart weight (mg)/Tibia lenght (mm)
p=0.06
ns
Ctrl AngII Ctrl AngII
DMSO Volasertib
e
AS
DIA
SR
Internal diameter (mm)
Ctrl AngII Ctrl AngII
DMSO Volasertib
f
Ascending aorta
Number of breaks/section
Abdominal aorta
Number of breaks/section
Ctrl AngII Ctrl AngII
DMSO Volasertib
DMSO
AngII
Volasertib
AngII + Volasertib
Abdominal aorta
g
AngII + DMSO
AngII + Volasertib
H&E
EVG

Figure 6